AFRRI Reports

1990

April

May

June

Defense Nuclear Agency

Armed Forces Radiobiology Research Institute

Bethesda, Maryland 20814-5145

Approved for public release; distribution unlimited

REPORT DOCUMENTATION PAGE

Form Approved
OMB No. 0704-0188

Public reporting burden for this collection of information is estimated to average 1 hour per response, including the time for reviewing instructions, searching existing data sources, gathering and maintaining the data needed, and completing and reviewing the collection of information. Send comments regarding this burden estimate or any other aspect of this collection of information, including suggestions for reducing this burden, to Washington Headquarters Services, Directorate for Information Operations and Reports, 1215 Jefferson Davis Highway, Suite 1204, Arlington, VA 22202-4302, and to the Office of Management and Budget, Paperwork Reduction Project (0704-0188), Washington, DC 20503

1. AGENCY USE ONLY *(Leave blank)*	2. REPORT DATE	3. REPORT TYPE AND DATES COVERED
	1990 July	Reprints/Technical

4. TITLE AND SUBTITLE

AFRRI Reports, Apr-Jun 1990

5. FUNDING NUMBERS

NWED QAXM

6. AUTHOR(S)

7. PERFORMING ORGANIZATION NAME(S) AND ADDRESS(ES)

Armed Forces Radiobiology Research Institute
Bethesda, MD 20889-5145

8. PERFORMING ORGANIZATION REPORT NUMBER

SR90-7 - SR90-10

9. SPONSORING/MONITORING AGENCY NAME(S) AND ADDRESS(ES)

Defense Nuclear Agency
Washington, DC 20305

10. SPONSORING/MONITORING AGENCY REPORT NUMBER

11. SUPPLEMENTARY NOTES

12a. DISTRIBUTION/AVAILABILITY STATEMENT

Approved for public release; distribution unlimited.

12b. DISTRIBUTION CODE

13. ABSTRACT *(Maximum 200 words)*

This volume contains AFRRI Scientific Reports SR90-7 through SR90-10 for Apr-Jun 1990.

14. SUBJECT TERMS

15. NUMBER OF PAGES
33

16. PRICE CODE

17. SECURITY CLASSIFICATION OF REPORT	18. SECURITY CLASSIFICATION OF THIS PAGE	19. SECURITY CLASSIFICATION OF ABSTRACT	20. LIMITATION OF ABSTRACT
UNCLASSIFIED	UNCLASSIFIED	UNCLASSIFIED	same as report

CONTENTS

Volume 261, number 1, 165–170 FEBS 08093 February 1990

Vanadyl-induced Fenton-like reaction in RNA

An ESR and spin trapping study

ARMED FORCES RADIOBIOLOGY RESEARCH INSTITUTE
SCIENTIFIC REPORT
SR90-7

Alasdair J. Carmichael

Radiation Biochemistry Department, Armed Forces Radiobiology Research Institute, Bethesda, MD 20814-5145, USA

Received 5 December 1989

Vanadyl (VO^{2+}) complexed to RNA reacts with hydrogen peroxide in a Fenton-like manner producing hydroxyl radicals ('OH). The hydroxyl radicals can be spin trapped with 5,5-dimethyl-1-pyrroline-1-oxide (DMPO) forming the DMPO-OH spin adduct. In addition, in the presence of ethanol the formation of the hydroxyethyl radical adduct of DMPO (DMPO-ETOH) confirms the production of hydroxyl radicals by the RNA/VO^{2+} complex. When the reaction between the RNA/VO^{2+} complex and H_2O_2 is carried out in the presence of the spin trap 2-methyl-2-nitrosopropane (MNP), radicals produced in the reaction of 'OH with RNA are trapped. Base hydrolysis of the MNP-RNA adducts (pH 12) followed by a reduction in the pH to pH 7 after hydrolysis is complete, yields an MNP adduct with a well-resolved ESR spectrum identical to the ESR spectrum obtained from analogous experiments with poly U. The ESR spectrum consists of a triplet of sextets ($a_N = 1.48$ mT, $a_N^\beta = 0.25$ mT and $a_H^\beta = 0.14$ mT), indicating that the unpaired nitroxide electron interacts with the nuclei of a β-nitrogen and β-hydrogen. The results suggest that the 'OH generated in the RNA/VO^{2+} reaction with H_2O_2 add to the C(5) carbon of uracil forming a C(6) carbon centered radical. This radical is subsequently spin trapped by MNP.

Vanadium; Vanadyl; Hydrogen peroxide; Hydroxyl radical; Electron spin resonance; Spin trapping

1. INTRODUCTION

The purpose of this work is to study, using ESR and spin trapping, vanadyl-induced Fenton-like reactions in RNA. Spin trapping is a technique by which a short-lived free radical is reacted with a spin trap, usually a nitrone or nitroso compound, to give a longer-lived nitroxide spin adduct which can be identified by ESR [1].

The oxycation of vanadium(IV), vanadyl (VO^{2+}), has proven to be an effective spin probe in biological systems [2–4]. Vanadyl has a single unpaired electron in its lowest nondegenerate vanadium d_{xy} orbital [5]. In a magnetic field, this electron interacts with the ^{51}V nucleus (99.7% abundant) which has a nuclear spin, $I = 7/2$, generating an isotropic ESR spectrum at room temperature consisting of 8 sharp lines [6]. However, when VO^{2+} is bound to a membrane component or to a slowly tumbling large molecule (protein, nucleic acid) in solution, it yields an anisotropic ESR spectrum. This spectrum resembles the ESR spectrum of immobilized vanadyl in a polycrystalline state or frozen solution [7]. The versatility of vanadyl as spin probe and its capacity to yield important information with regard to metal properties in biological systems, is due mainly to this susceptibility of the vanadyl ESR spectrum to the motion of the cation in solution.

Other aspects of the VO^{2+} chemistry are also of interest in biology. Similar to Fe(II) and Cu(I), VO^{2+} participates in Fenton-like reactions reacting with H_2O_2 to produce hydroxyl radicals ('OH) [8–11]. Using vanadyl ESR, Brooks et al. [8] studied the kinetics of this reaction. Recently, Keller et al. [9,10] using spin trapping have studied the effects of vanadyl on lipid peroxidation and oxidation of NADH. In both studies vanadyl-induced 'OH were implicated. Also, using spin trapping in aqueous solutions of VO^{2+} and Fe^{2+} salts, Carmichael [11] has shown that VO^{2+} generates, in a Fenton-like reaction, approximately half the 'OH as compared to FE^{2+}. This does not necessarily have to be the case when the reactions occur in biological systems. In biological systems these metals are complexed and may contain a large variety of ligands that could possibly alter their chemical properties.

An increasing interest has developed with regard to the role of metal ions in nucleic acid damage [12]. However, most of the emphasis has been placed on Fenton-driven iron and copper reactions. Vanadyl forms complexes with nucleic acids (RNA, DNA) and with ribonucleosides [13–16]. The effects of vanadyl-ribonucleoside complexes on enzymes important to recombinant DNA technology are well documented [14–16]. Therefore, since it is possible that vanadyl may be associated in some manner (still unclear) with nucleic acids in the cell, knowledge of the chemistry of these

Correspondence address: A.J. Carmichael, Radiation Biochemistry Department, Armed Forces Radiobiology Research Institute, Bethesda, MD 20814-5145, USA

Published by Elsevier Science Publishers B.V. (Biomedical Division)
00145793/90/$3.50 © 1990 Federation of European Biochemical Societies

vanadyl-nucleic acid complexes is important. For this reason, in the present study VO^{2+}/RNA complexes were reacted with H_2O_2 in order to determine their capacity to generate ·OH in a Fenton-like manner. In addition, it is of interest to determine the fate of the ·OH following their formation.

2. MATERIALS AND METHODS

Vanadyl sulfate was obtained from Fisher Scientific Co. (Fair Lawn, NJ). The concentration of vanadyl was determined spectrophotometrically (λ = 750 nm, ϵ = 18 $M^{-1}\cdot cm^{-1}$) [17]. Hydrogen peroxide was obtained from Sigma (St. Louis, MO) and its concentration was determined by titration with potassium permanganate [18]. The spin traps 5,5-dimethyl-1-pyrroline-1-oxide (DMPO) and 2-methyl-2-nitrosopropane (MNP) were purchased from Aldrich (Milwaukee, WI). DMPO was purified following the method of Buettner and Oberley [19]. In this method, DMPO is successively treated with activated charcoal until all free radical impurities are eliminated as verified by ESR. The concentration of DMPO was measured spectrophotometrically (λ = 227 nm, ϵ = 8 × 10^3 $M^{-1}\cdot cm^{-1}$) [20]. MNP (3–5 mg/ml) was dissolved in water by stirring in the dark at 45°C as described by Makino et al. [21]. The spin trap 3,5-dibromo-4-nitrosobenzenesulfonic acid (DBNBS) was purchased from Sigma and was used without further purification by dissolving directly in water at the desired concentration. Metal-free water was used in all solutions. This water was prepared by further treating, in a separating funnel, water obtained from a Sybron/Barnstead NANO pure system with a 0.001% dithizone (Sigma) solution in carbon tetrachloride. The water was heated to boiling in a water bath in order to eliminate all residual organic material. All glassware was kept permanently soaking in a 1:1 mixture of sulfuric and nitric acids to eliminate trace metals. Immediately prior to use, the glassware was rinsed with metal-free water and dried under a stream of nitrogen.

Calf liver RNA, poly A, poly C, poly G and poly U were purchased from Sigma. The polynucleotides were used as standards and model systems for RNA. To eliminate any metals bound to these nucleic acids, solutions of RNA and polynucleotides were dialyzed, first against several changes (volume ratio 1:250) of 0.01 M EDTA and then, against several changes of metal-free water to eliminate the EDTA. The nucleic acid solutions were then lyophilized and stored until required.

For experiments requiring DMPO, this spin trap was added (0.1 M final) to a 1:1 mixture of VO^{2+}/nucleic acid (1 × 10^{-3} M) followed by addition of H_2O_2 (1 × 10^{-3} M). To avoid chelation of VO^{2+} by MNP in the experiments requiring this spin trap, the MNP was mixed with the H_2O_2 and added to the VO^{2+}/nucleic acid solution. Except for MNP which had a final concentration of 2.5 × 10^{-2} M, the concentration of all other species in the MNP experiments was the same as in the experiments requiring DMPO. The solutions containing the MNP-nucleic acid spin adducts were immediately extracted with petroleum ether to eliminate any ditertiary butyl nitroxide (d-tBN) impurity which may be formed and is frequently generated in experiments with MNP [22]. The solutions were then purged with nitrogen to eliminate any residual petroleum ether. In addition, the petroleum ether extraction and the nitrogen bubbling also eliminate all the excess or unreacted MNP due to the higher solubility of this spin trap in nonpolar solvents and its volatility.

The spin-trapped nucleic acids were subjected to base hydrolysis (pH 12) with dilute NaOH. Once the hydrolysis was complete as judged by the resolution of the ESR spectra, the pH of the solutions were lowered to pH 7 and the final ESR spectra were recorded. ESR spectra were also recorded immediately after addition of the H_2O_2. The ESR spectra were recorded on a Varian E-109 spectrometer at 100 kHz magnetic field modulation. The instrument was set at a magnetic field: 3700 G (for VO^{2+}), 3350 G (for spin adducts); microwave frequency: 9.510 GHz; microwave power: 10 mW; modulation amplitude: 10 G (for VO^{2+}), 0.5 G (for spin adducts); scan range: 2000 G (for VO^{2+}), 100 G (for spin adducts); and unless otherwise specified, the time constant and scan times were 0.25 s and 4 min, respectively. Spectral parameters were obtained by computer simulation, generating theoretical ESR spectra that best match the experimental ESR spectra.

3. RESULTS AND DISCUSSION

When vanadyl sulfate (1 × 10^{-3} M) is mixed with H_2O_2 (1 × 10^{-3} M) in the presence of DMPO (0.1 M), the ESR spectrum shown in fig.1A is obtained. This spectrum consists of the typical isotropic 8-line VO^{2+} spectrum superimposed by another ESR spectrum consisting of 4 sharp lines. Reducing the instrument scan range from 2000 G to 100 G and the modulation amplitude from 10 G to 0.5 G, these additional 4 lines become well resolved into the 1:2:2:1 pattern shown in fig.1B. This ESR spectrum with hyperfine coupling constants, $a_N = a_H^\beta$ = 1.49 mT, corresponds to the DMPO-OH spin adduct [23]. Since DMPO-OH may be formed by pathways other than the direct addition of ·OH to DMPO, an experiment was done reacting vanadyl sulfate (1 × 10^{-3} M) with H_2O_2 (1 × 10^{-3} M) in the presence of D,L-histidine (1 × 10^{-2} M) and the spin trap MNP (1 × 10^{-2} M) in order to verify the generation of ·OH. The spin adduct produced in this reaction yields an ESR spectrum (fig.1C) in which each line in the primary nitroxide triplet is split into 12 lines in a 1:1:2:2:3:3:3:3:2:2:1:1 pattern. This pattern is obtained when the unpaired nitroxide electron interacts with the nuclei of a nitrogen and 3 hydrogens from the histidine molecule. Fig.1D shows the computer simulation that matches the experimental ESR spectrum (fig.1C). This computer simulation was generated using hyperfine coupling values of 1.52 mT, 0.19 mT, 0.38 mT, 0.19 mT and 0.073 mT for the primary nitroxide nitrogen, the histidine nitrogen and the 3 histidine protons, respectively. These hyperfine coupling constants are consistent with the known spectral parameters for the histidyl radical adduct of MNP formed following ·OH reaction with histidine [24]. In addition, when higher concentrations (0.1 M) of D,L-histidine are used and the reaction is carried out at pH 7, the spin adduct obtained is predominantly a triplet of doublets with hyperfine coupling constants a_N = 1.57 mT and a_H^β = 0.34 mT. These values are also consistent with previous data obtained for the spin trapping of histidyl radicals following the reaction of ·OH with histidine [24]. The results shown in fig.1 confirm that ·OH are formed at the concentrations of VO^{2+} and H_2O_2 used.

Although solutions of vanadyl salts react with H_2O_2 generating ·OH, the question still remains whether this cation bound to a large biological molecule, such as a nucleic acid, will react in the same manner. Therefore, VO^{2+} (1 × 10^{-3} M) chelated to RNA (1 × 10^{-3} M) was mixed with H_2O_2 (1 × 10^{-3} M) in the presence of the

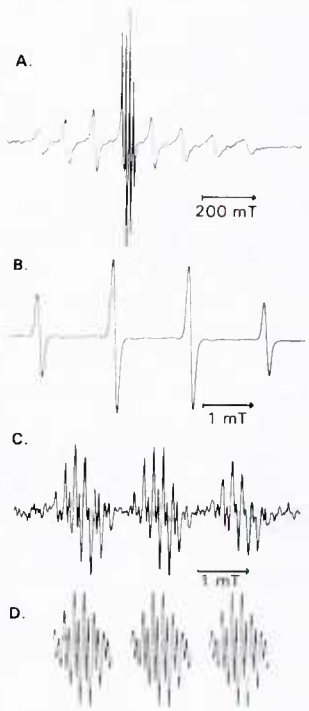

Fig.1. (A) ESR spectrum of $VOSO_4$ (1×10^{-3} M) following its reaction with H_2O_2 ($\times 10^{-3}$ M) in the presence of DMPO (0.1 M). (B) DMPO-OH ESR spectrum observed in the center region of (A) after reducing the instrument microwave power, modulation amplitude and scan range. (C) ESR spectrum of the MNP-histidyl adduct from the reaction of $VOSO_4$ with H_2O_2 (same concentrations as in (A)) in the presence of histidine (1×10^{-3} M) and MNP (2.5×10^{-2} M). (D) Computer simulation of the ESR spectrum in (C). Instrument receiver gain was set at: 1.25×10^4, 2×10^3 and 1.6×10^5 for (A), (B) and (C), respectively. The time constant and scan time for (C) were 2 s and 30 min, respectively.

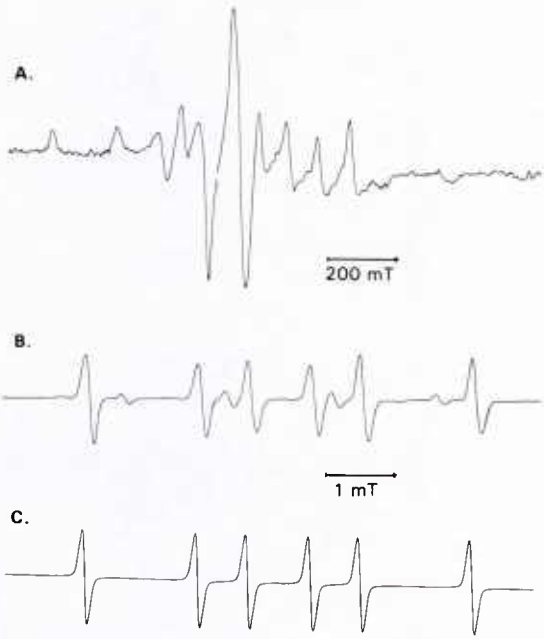

Fig.2. (A) ESR spectrum of VO^{2+} (1×10^{-3} M) bound to RNA (1×10^{-3} M) in the presence of DMPO (0.1 M). (B) ESR spectrum of DMPO-hydroxyethyl adduct following reaction of mixture in (A) with H_2O_2 (1×10^{-3} M) in the presence of ethanol (1.7 M). (C) Computer simulation of ESR spectrum in (B). Instrument receiver gain was set at: 2×10^4 and 2.5×10^3 for (A) and (B), respectively.

spin trap DMPO (0.1 M). Fig.2 shows the results of this experiment. Fig.2A is the typical anisotropic ESR spectrum obtained from immobilized VO^{2+} when bound to a large slowly tumbling molecule in solution [25]. This spectrum was obtained in the presence of DMPO and therefore, shows that all VO^{2+} remains bound to the nucleic acid in the presence of this spin trap. In order to verify that the VO^{2+}/RNA complex does generate ·OH when mixed with H_2O_2, the reaction was carried out in the presence of ethanol (1.7 M). The predominant spin adduct formed (fig.2B) consists of a triplet of doublets and can be computer-simulated using hyperfine coupling constants, $a_N = 1.58$ mT, $a_H^\beta = 2.28$ mT (fig.2C). These spectral parameters are consistent with those previously reported for DMPO-hydroxyethyl radical formed following the reaction of ·OH with ethanol [23]. Although at the concentration of ethanol used all ·OH formed should react with this reagent, the additional ESR lines observed in fig.2B show that a small fraction of DMPO-OH is also formed. The formation of this additional DMPO-OH has previously been observed in Fenton-like reactions involving VO^{2+} and possibly originates from the oxidation of DMPO by a reactive vanadium intermediate [11].

It is of interest to determine whether the ·OH generated by the VO^{2+}/RNA complex react with RNA itself. Therefore, solutions of the VO^{2+}/RNA complex, prepared in a similar fashion to the previous experiments, were mixed with H_2O_2 (1×10^{-3} M) in the presence of the spin trap MNP (2.5×10^{-2} M). However, in this experiment the H_2O_2 and MNP were added simultaneously as a mixture to the VO^{2+}/RNA solution. This was done in order for the reaction to occur instantaneously at the RNA molecule and to avoid chelation of VO^{2+} by MNP which occurs when MNP is mixed with VO^{2+}/RNA prior to the addition of H_2O_2. Fig.3A shows the ESR spectrum of the VO^{2+}/RNA complex. Addition of the H_2O_2 and MNP mixture to the solution containing the VO^{2+}/RNA complex, causes the disappearance of the VO^{2+}/RNA ESR spectrum and yields the sharp 3-line ESR spectrum shown in fig.3B. Reducing the instrument scan range and the modulation amplitude in a similar fashion as shown in fig.1, the ESR spectrum in fig.3B becomes better resolved showing 3 broad lines (fig.3C) typical of a nitroxide radical partially immobilized by a large molecule in solution. This result indicates that ·OH produced in the reaction between VO^{2+}/RNA and H_2O_2 react with RNA generating nucleic acid radicals which are spin trapped by MNP.

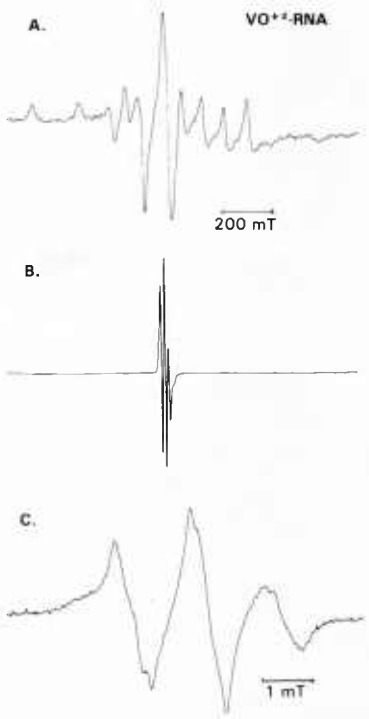

Fig.3. ESR spectra of: (A) VO^{2+}/RNA complex; (B) following reaction of VO^{2+}/RNA with H_2O_2 (1×10^{-3} M) in the presence of MNP (2.5×10^{-2} M); (C) spin-trapped RNA (same as in (B)) after reducing the instrument modulation amplitude and scan range. Instrument receiver gain was set at: 2×10^4 for (A) and (C); 2×10^3 for (B).

To determine the location of the trapped radicals in the RNA molecule, the spin-trapped RNA was hydrolyzed (pH 12) with dilute sodium hydroxide. Because the ribose sugars in RNA contain a 2′-hydroxyl group this nucleic acid is susceptible to base hydrolysis [26]. This method is effective for hydrolyzing spin-trapped RNA because it is strictly chemical and it avoids any specificity complications that could occur, due to the bound spin trap, during enzymatic hydrolysis with RNase. It must be noted that base hydrolysis is not completely free of complications in spin trapping experiments of the nature described in this work using MNP. Control experiments using polynucleotides show that at pH 12 and only in the presence of MNP, polynucleotides yield identical spin adducts as those obtained following their reaction with ·OH. However, this problem can be circumvented by extracting the solutions with petroleum ether and bubbling with nitrogen immediately prior to raising the pH to pH 12. MNP is volatile and is more soluble in nonpolar solvents than in water. Therefore, petroleum ether extraction not only eliminates any ditertiary butyl nitroxide (d-tBN), an impurity frequently formed in experiments with MNP [22], it also eliminates the excess unreacted MNP. Nitrogen bubbling through the samples eliminates the residual MNP remaining in the solution and also the residual petroleum ether. Following these precautions, the hydrolysis products observed by ESR originate only from the spin trapped nucleic acids formed subsequently to their reaction with ·OH. Once the hydrolysis at pH 12 of the spin-trapped RNA is complete, the resolution of the broad ESR spectrum (fig.3C) increases permitting the identification of the spin adducts. Fig.4A shows the ESR spectrum of the hydrolyzed spin-trapped RNA after reducing the pH to pH 7. This spectrum consists of a triplet of sextets indicating that the unpaired nitroxide electron is interacting with the nuclei of a secondary nitrogen and a secondary hydrogen. The computer-generated theoretical spectrum that best matches the experimental spectrum (fig.4A) is shown in fig.4B). This simulation was obtained using the hyperfine coupling constants, a_N = 1.48 mT, a_N^β = 0.25 mT and a_H^β = 0.14 mT. Since all bases in RNA contain at least one position where addition of MNP would permit the interaction of the unpaired nitroxide electron with the nuclei of a β-nitrogen and β-hydrogen, similar experiments to the VO^{2+}/RNA reaction with H_2O_2 were carried out using poly A, poly C, poly G and poly U as model systems and standards for RNA. Fig.4C shows the ESR spectrum (pH 7) of the spin adduct obtained from the hydrolysis of the spin-trapped poly U. This spectrum is identical to the spectrum obtained from the RNA experiment (fig.4A) and is matched by the computer simulation (fig.4B). The only position in uracil that addition of MNP would produce an ESR spectrum consisting of a triplet of sextets is the C(6) carbon. Therefore, the results show that following the reaction of VO^{2+}/RNA complex with H_2O_2 only radicals at the C(6) uracil carbon were spin trapped. This result is consistent with the results obtained following γ-radiolysis of RNA solutions containing MNP (28). Although hydrolysis of the spin trapped poly C also yields a spin adduct (pH 7) with ans ESR spectrum consisting of a triplet of sextets with hyperfine coupling constants, a_N = 1.49 mT, a_N^β = 0.27 mT and a_H^β = 0.16 mT, this spectrum is different to the ESR spectra of the spin adducts originating from RNA and poly U. In experiments with poly A, the ESR spectrum was lost when reducing the pH to pH 7. However, at pH 12 the ESR spectrum for hydrolyzed spin-trapped poly A is different from the ESR spectrum for the hydrolyzed spin-trapped RNA. This suggests that in RNA no adenine radicals were spin trapped. In experiments using poly G no radicals were spin trapped. Therefore, it is possible that in the RNA experiments guanine radicals may have been formed but were not observed by spin trapping.

There are 4 immediate reasons that could possibly explain the spin trapping of RNA radicals only at the uracil C(6) position: (1) vanadyl binds to RNA regions rich in uracil; (2) the stability of spin adducts for different bases is not equal; (3) ·OH reacts with all bases followed by spin density migration to uracil; and (4) the MNP spin trapping efficiency is not equal for radicals produced in different bases. It must be noted that ·OH will react at approximately equal rates with all RNA

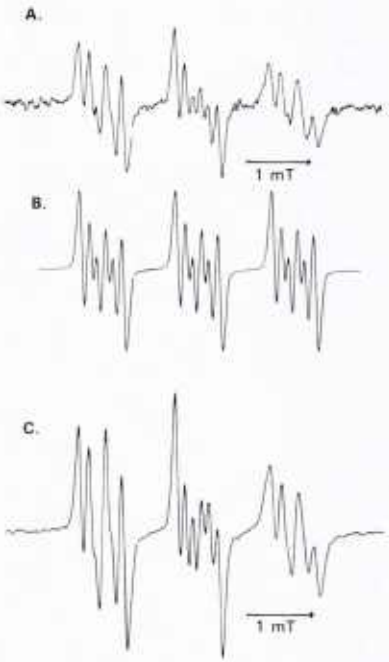

Fig.4. ESR spectra at pH 7 obtained after base hydrolysis (pH 12) of solutions containing MNP-RNA spin adduct (A) and MNP-poly U spin adduct (C). Computer simulation of these spectra is shown in (B). Instrument receiver gain was set at: 5×10^4 and 2×10^4 for (A) and (C), respectively. Both spectra were recorded with 8 min scan time and 0.5 s time constant.

bases [27].

It is unlikely that VO^{2+} binding to RNA regions rich in uracil can be the cause of the observed results. Identical results are obtained in spin trapping experiments with RNA using γ-radiolysis as the source of $^{\cdot}OH$ [28]. Furthermore, in this case experiments were also done using different sources of RNA (calf liver and bakers yeast) to insure base composition variability. The stability of the spin adducts is also an unlikely reason for observing only a uracil adduct in the RNA experiments. Although the results from the poly A experiments may suggest that spin adduct stability plays a role in the observed RNA results, it is improbable because the stability of the sping adducts originating from poly C and poly U is equal, yet no cytosine spin adducts are observed in the RNA experiments.

It is conceivable that an intramolecular mechanism may exist by which following $^{\cdot}OH$ reaction with any of the RNA bases, the radical spin density may migrate to its most stable location in the nucleic acid prior to its reaction with MNP. In this case, the results suggest the C(6) carbon of uracil. However, this cannot be definitely concluded without prior knowledge of the MNP spin trapping efficiency for radicals formed on all RNA bases. As estimated from the intensity of the spin adduct ESR spectra, the MNP spin trapping of radicals formed in poly U is approximately twice and 5 times more efficient than for poly C and poly A, respectively. If this observation can be extrapolated to the RNA case, the results may suggest that in RNA spin trapping of base radicals by MNP occurs preferentially at uracil followed by cytosine, adenine and guanine. No observed spin trapping results in the experiments using poly G suggest low spin trapping efficiency by MNP for poly G radicals. In an attempt to determine whether other base radicals could be spin trapped in RNA, similar experiments were done using another nitroso spin trap, DBNBS, instead of MNP. However, in these experiments the intensity of the ESR spectrum of the spin-trapped RNA was much lower compared to the ESR spectrum of RNA spin-trapped by MNP. Furthermore, the DBNBS spin-trapped RNA was not stable and decomposed during hydrolysis at pH 12.

In conclusion, although the results appear to favor spin trapping efficiency as the major reason in RNA for observing only spin-trapped uracil at the C(6) carbon, it must be noted that certain experimental facts favor an intramolecular spin density migration mechanism. For instance, the concentration of MNP (2.5×10^{-2} M) in the experiments was sufficiently high to allow trapping of any base radical formed. The total amount of base radicals that can be formed cannot surpass the concentration of $^{\cdot}OH$ generated. In turn, the concentration of $^{\cdot}OH$ formed is limited by the initial VO^{2+} and H_2O_2 concentrations (1×10^{-3} M). It should be expected that a 25-fold excess of MNP would offset any of the differences in MNP spin trapping efficiencies observed for polynucleotide radicals.

REFERENCES

[1] Janzen, E.G. (1980) in: Free Radicals in Biology, vol. 1V (Pryor, W.A., ed.) pp. 115–154, Academic Press, New York.
[2] Chasteen, N.D. (1981) in: Biological Magnetic Resonance, vol. 3 (Berliner, L. and Rueben, L., eds) pp. 53–119.
[3] Chasteen, N.D. (1983) Structure and Bonding 53, 105–138.
[4] Boyd, W.D. and Kustin, K. (1984) Advances in Inorganic Biochemistry 6, 311–365.
[5] Balhausen, C.J. and Grey, H.B. (1962) Inorg. Chem. 1, 111–122.
[6] Francavilla, J. and Chasteen, N.D. (1975) Inorg. Chem. 14, 2860–2862.
[7] Albanese, N.F. and Chasteen, N.D. (1978) J. Phys. Chem. 82, 910–914.
[8] Brooks, H.B. and Sicilio, F. (1971) Inorg. Chem. 10, 2530–2534.
[9] Keller, R.J., Sharma, R.P., Grover, T.A. and Piette, L.H. (1988) Arch. Biochem. Biophys. 265, 524–533.
[10] Keller, R.J., Coulombe jr, R.A., Sharma, R.P., Grover, T.A. and Piette, L.H. (1989 Free Radical Biol. Med. 6, 15–22.
[11] Carmichael, A.J., (1989) Free Radical Res. Commun. in press.
[12] Beaumont, P.C. and Deeble, D.J. (1989) Int. J. Radiat. Biol. 55, 157–161.
[13] Snipes, W. and Gordy, W. (1964) J. Chem. Phys. 41, 3661–3662.
[14] Puskas, R.S., Nanley, N.R., Wallace, D.M. and Berger, S.L. (1982) Biochemistry 21, 4602–4608.
[15] Schulz-Harder, B. and Tata, J.R. (1982) Biochem. Biophys. Res. Commun. 104, 903–910.
[16] Talib, S. and Hearst, J.E. (1983) Nucleic Acids Res. 11, 7031–7042.

[17] Fitzgerald, J.J., and Chasteen, N.D. (1974) Anal. Biochem. 60, 170–180.
[18] Kolthoff, I.M., Sandell, E.B., Meehan, E.J. and Brukenstein, S. (1969) in: Quantitative Chemical Analysis (4th edn) p. 834, Macmillan.
[19] Buettner, G.R. and Oberley, L.W. (1978) Biochem. Biophys. Res. Commun. 83, 69–74.
[20] Kalyanaraman, B., Felix, C.C. and Sealy, R.C. (1982) Photochem. Photobiol. 36, 5–12.
[21] Makino, K., Suzuki, N., Moriya, F., Rokushika, S. and Hatano, H. (1981) Radiat. Res. 86, 294–310.
[22] Rustgi, S. and Riesz, P. (1978) Radiat. Res. 75, 1–17.
[23] Buettner, G.R. (1987) Free Radical Biol. Med. 3, 259–303.
[24] Rustgi, S., Joshi, A., Moss, H. and Riesz, P. (1977) Int. J. Radiat.. Biol. 31, 415–440.
[25] Carmichael, A.J. and Vincent, J.S. (1979) FEBS Lett. 105, 349–352.
[26] Lehninger, A.L. (1975) in: Biochemistry (2nd edn) p. 322, Worth, New York.
[27] Dorfman, L.M. and Adamms, G.E. (1973) in: NSRDS 46, US Government Printing Office, Washington, DC.
[28] Carmichael, A.J., Arroyo, C.M. and Walden, T.L. (1989) in: Oxygen Radicals in Biology and Medicine (Simic, M.G., Taylor, K.A., Ward, J.F. and von Sonntag, C., eds) pp. 437–439, Plenum, New York.

ARMED FORCES RADIOBIOLOGY RESEARCH INSTITUTE
SCIENTIFIC REPORT
SR90-8

Alterations in Rat Cardiac Myosin Isozymes Induced by Whole-Body Irradiation Are Prevented by 3,5,3'-L-Triiodothyronine

Raye Z. Litten, Henry G. Fein, Grealon T. Gainey, Thomas L. Walden, and Robert C. Smallridge

Changes in cardiac myosin isozymes and serum thyroid hormone levels were investigated in rats following 10 Gy whole-body gamma irradiation. The percent β-myosin heavy chain increased from 21.3 ± 1.8 to 28.1 ± 6.8 (NS) at 3-day postirradiation, 37.7 ± 1.9 ($P < .001$) at 6-day postirradiation, and 43.8 ± 3.3 ($P < .001$) at 9-day postirradiation. Along with the change in myosin isozymes was a significant 53% decrease ($P < .001$) in the serum thyroxine (T_4) level by day 3 postirradiation, remaining depressed through day 9 postirradiation. The serum 3,5,3'-triiodothyronine (T_3) level, however, was normal until day 9, when significant depression was also observed. In contrast, the thyroid-stimulating hormone (TSH) level was significantly increased by fourfold at day 3, returning to near normal values by day 9 postirradiation. Daily injections of physiological doses of T_3 (0.3 μg/100 g body weight) prevented the change in the myosin isozymes following whole-body irradiation. Daily pharmacological injections of T_3 (3.0 μg/100 g body weight) to the irradiated rats produced a further decrease in the percent β-myosin heavy chain (below control values) indicating tissue hyperthyroidism. Thus, this study suggests that the change in myosin isozymes following whole-body irradiation is caused by an alteration in thyroid hormone activity.

This is a US government work. There are no restrictions on its use.

THREE TYPES of cardiac myosin isozymes have been shown to exist within the ventricle of the heart: V_1, V_2, and V_3. V_1 contains two alpha (α)-heavy chains, whereas V_3 consist of two beta (β) chains.[1-3] V_2, which is a minor component, is a heterodimer composed of one α- and one β-heavy chain.[4,5]

The relative proportions of the cardiac myosin isozymes change under various conditions. There is a shift toward V_3 isozyme with an increase in age as well as cardiac hypertrophy induced by pressure overload.[6-9] In addition, the thyroid hormones have exerted a strong influence in changing the V_3/V_1 ratio within the ventricle by regulating the transcription rate of the α- and β-myosin heavy chains.[10] Under conditions of hypothyroidism, there is an increase in the amount of β-heavy chain (V_3) and a decrease in the α-heavy chain (V_1), while under the conditions of hyperthyroidism the opposite occurs.[9,11] A similar increase in V_3 isozyme occurs with long-term semistarvation.[12]

Changes in the relative amounts of V_1 and V_3 isozymes have been shown to alter cardiac performance. V_1 isozyme has a higher actin- and calcium-stimulated adenosine triphosphatase (ATPase) activity than does the V_3 isozyme.[1,3] A high proportion of V_3 isozyme is associated with relatively slow, but economic force development within the heart, while a high proportion of V_1 is associated with a faster, but less economical force development.[13]

Recently, we have shown that whole-body gamma irradiation of rats causes a shift toward the V_3 isozyme 9 and 30 days postirradiation.[14] In this study, we examined early changes in the myosin isozymes at 3, 6, and 9 days postirradiation. We also measured the serum levels of T_4, T_3, and thyroid-stimulating hormone (TSH) to see if a relationship exists between thyroid hormones and cardiac myosin isozymes. Finally, T_3 was injected into the irradiated rats to see if changes in the myosin isozymes could be prevented.

MATERIALS AND METHODS

Animal Model

Three-month-old male Sprague Dawley rats (Harlan, Indianapolis, IN) were quarantined for a period of 2 to 3 weeks and determined to be free of pathological and serological illness and infection. The rats were housed three to a cage in Micro-isolator cages on hardwood chip bedding and maintained in conventional animal holding rooms on a 12-hour light-dark cycle. The rooms were maintained at 21° ± 1°C with 50% relative humidity and 12 room changes of 100% conditioned fresh air per hour. Wayne Rodent Blox dietary pellets (Continental Grain Co, Chicago, IL) and acidified water (pH 2.4) were provided ad libitum.

For whole-body irradiation, rats were placed in individual plastic rectangular cages and irradiated with a bilateral cobalt-60 source at a dose rate of 40 Gy/min for total of 10 Gy. One hundred-percent lethality occurs in approximately 12 days after the radiation exposure. In the T_3 injection studies, rats received eight daily intraperitoneal (IP) injections of T_3 (Sigma Chemical Co, St Louis, MO) beginning at the time of irradiation at a physiological dose of 0.3 μg/100 g body weight[15] or a pharmacologic dose of 3.0 μg/100 g body weight. Age-matched rats were used as controls.

Rats were anesthetized with a combination of ketamine (Vetalar, Parke-Davis, Morris Plains, NJ) and xylazine (Rompun; Haver, Shawnee, KS) (8:1, 45 mg per Kg body weight, IM) until death was achieved. Blood was removed by cardiac puncture and centrifuged at 2,500 × *g* for 20 minutes. The serum was stored at −80°C until T_4,

From the Departments of Physiology and Biochemistry, Armed Forces Radiobiology Research Institute, Bethesda, MD. and the Division of Medicine, Walter Reed Army Institute of Research, Washington, DC.

Supported by the Armed Forces Radiobiology Research Institute, Defense Nuclear Agency, Department of the Army, and Department of Defense, under Research Work Unit 0169.

The views presented in this paper are those of the authors. No endorsement by the Defense Nuclear Agency and the Department of Defense has been given or should be inferred.

Research was conducted according to the principles enunciated in the "Guide for the Care and Use of Laboratory Animals," prepared by the Institute of Laboratory Animal Resources, National Research Council.

Address reprint requests to R.Z. Litten, PhD, Room 16C-05, Division of Clinical and Prevention Research, National Institute on Alcohol Abuse and Alcoholism. Parklawn Bldg. Rockville, MD 20857.

This is a US government work. There are no restrictions on its use.

0026-0495/90/3901-0010$0.00/0

T_3, and TSH were measured (see below). The heart was then immediately removed and the apex region of the left ventricle frozen at −80°C for pyrophosphate gel electrophoresis (see below). In certain cases, the remaining heart tissue was fixed in 10% formalin for histological examination. After embedding the tissue in paraffin, tissue slices were obtained with a microtome and stained with either hematoxylin-eosin or Masson's stain.

Pyrophosphate Gel Electrophoresis

Cardiac myosin was extracted by homogenization of frozen left ventricular apex in 100 mmol/L sodium pyrophosphate, pH 8.8, 5 mmol/L EDTA, 2 mmol/L 2-mercaptoethanol, and 0.2 mmol/L dichlorvos. Pyrophosphate gel electrophoresis was carried out as previously described.[8] The gels were then scanned and quantitated with a LKB Ultrascan Laser Densitometer (Shell, Houston, TX) (Fig 1). The amount of the heterodimer V_2, which is a minor component, was divided equally between V_3 and V_1, and expressed as percent β and percent α myosin heavy chain.

Serum Measurements

Serum T_3 and T_4 were measured using radioimmunoassay (RIA) kits (Gamma Coat; Baxter Healthcare Corp, Cambridge, MA). Serum TSH was measured using reagents provided by National Hormone and Pituitary Program, National Institute of Diabetes, Digestive, and Kidney Diseases. Free levels of T_3 and T_4 were determined by equilibrium dialysis (Nichols Institute, San Juan Capistrano, CA).

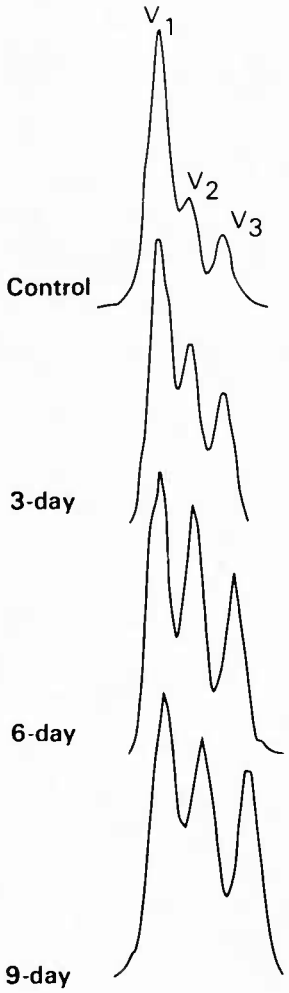

Fig 1. Densitometric traces of pyrophosphete gels of cardiac myosin isozymes (each gel loaded with 2 to 4 μg of myosin) from ege-matched control, 3-day, 6-dey, end 9-dey postirrediation (10 Gy) preparations. Similar separetions were obteined for ell semples in this study.

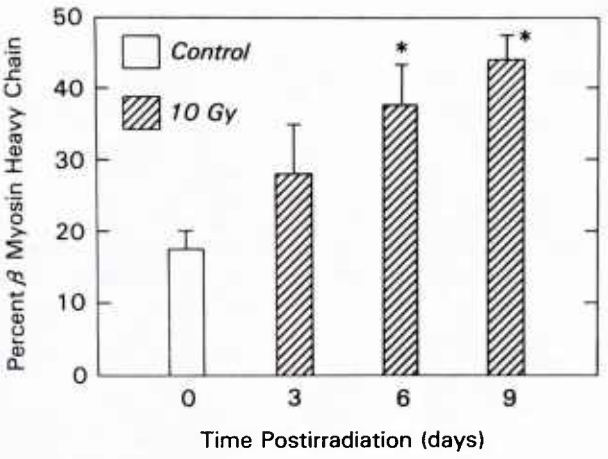

Fig 2. Percent β-myosin heavy chain from age-matched control, and 3-day, 6-day, and 9-dey postirradiated hearts. Values are mean ± SE for six to 17 hearts per group. There was no difference in the age-matched controls when enalyzed 3, 6, or 9 days post-irrediation end thus, the control values were pooled together. *$P <$ .001 versus aged-matched control velues.

Statistics

Statistical comparisons of control group with 3-, 6-, 9-day postirradiated groups were carried out using nonpaired Student's t tests with the Bonferroni correction for multiple comparisons. Wilcoxon rank sum test was used to compare the free level and percent dialyzable fraction of T_4 and T_3 in control and day 9 postirradiated groups.

RESULTS

Measurement of the percent β-myosin heavy chain was carried out in rat hearts 3, 6, and 9 days following 10 Gy whole-body gamma irradiation. The percent β-heavy chain increased from 21.3 ± 1.8 (SE) in aged-matched controls to 28.1 ± 6.8 (NS) 3 days postirradiation, 37.7 ± 1.9 ($P < .001$) 6 days postirradiation, and 43.8 ± 3.3 ($P < .001$) 9 days postirradiation (Figs 1 and 2).

Since thyroid hormone has been shown to alter the cardiac myosin isozymes, the serum T_4 and T_3 levels were measured in the irradiated rats. We found a significant depression in the serum T_4 levels 3, 6, and 9 days postirradiation (Fig 3A). However, there was no change in the serum levels of T_3 until day 9 postirradiation at which time a significant depression was observed (Fig 3B). To determine if the depressed levels of T_4 and T_3 (at day 9) were caused by alterations to thyroid binding proteins, we measured the free levels and the percent dialyzable fraction of T_4 and T_3 at day 9 postirradiation. We found a decrease in both free levels of T_4 (1.8 ± 0.4 *v* 2.4 ± 0.1 ng/dL, control; $P < .05$) and T_3 (284 ± 48 *v* 653 ± 35 pg/dL, control; $P < .001$). In addition, the percent dialyzable T_4 was increased in irradiated rats (0.063% ± 0.006% *v* 0.040% ± 0.002%, control; $P < .02$), indicating an additional effect on protein binding. For T_3, the dialyzable fraction was unaltered (0.791% ± 0.030% *v* 0.859% ± 0.020%, control; NS).

In addition to the T_3 and T_4 measurements, the serum

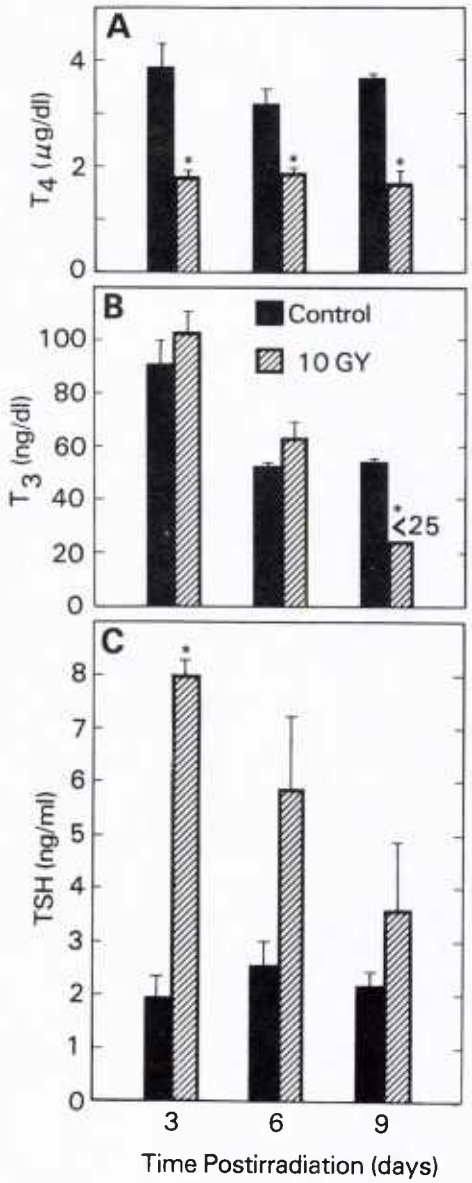

Fig 3. Serum levels of T_4(A), T_3(B), end TSH(C) of ege-matched controls versus 3-day, 6-day, end 9-dey postirredietion. Values are meen ± SE for five to nine animals per group. *$P < .001$ versus eged-matched control values.

TSH level was determined. We found that the TSH level was elevated fourfold on day 3 postirradiation, returning to near normal values at day 9 postirradiation (Fig 3C).

Since whole-body irradiation resulted in an increase in the percent β-myosin heavy chain as well as a decrease in the thyroid hormone level, we injected irradiated rats with T_3 to see if this could prevent and reverse the shift in the myosin isozymes. We observed that daily physiological injections of T_3 prevented the change in the percent β-myosin heavy chain in the irradiated rats, whereas daily pharmacologic injections of T_3 resulted in a shift to almost all α-myosin heavy chain (Fig 4). The serum level of T_4 remained depressed in the irradiated animals receiving the physiological and pharmacologic doses of T_3 (data not shown).

Finally, histological examination of the hearts from the irradiated rats and irradiated rats with T_3 daily injections showed no evidence of heart damage. There was no increase in fibrosis or any apparent gross changes in the structure of the myocardial cells.

DISCUSSION

Whole-body irradiation results in a change in the cardiac myosin isozymes shifting toward an increase in the β-myosin heavy chain. Along with this change in the myosin isozymes is a decrease in the serum level of thyroid hormones. Since it has been previously shown that hypothyroidism causes an increase in the β-myosin heavy chain,[1,16,17] the depressed thyroid hormone level may be responsible, in part, for the change in the myosin isozymes. This is further suggested by the T_3 injection study, which prevented the shift toward the β-myosin heavy chain following whole-body irradiation. Thus, it appears that the whole-body irradiation causes, either directly or indirectly, a decrease in the serum T_4 levels, which leads to an increase in the β-myosin heavy chain.

Change in the myosin isozymes has been associated with changes in cardiac function. V_3 myosin (β-heavy chain) has a relatively low calcium- and actin-stimulated ATPase activity, while the V_1 myosin (α-heavy chain) has a high ATPase activity.[3] A heart having a high V_3 content has a decrease in velocity of unloaded shortening and rate of isometric tension development and an increase in the economy of force development when compared with a heart with a high V_1 content.[13,18] Thus, a shift toward the V_3 isozyme following whole-body irradiation suggests that the contractile proteins of the heart contract slower but more economically.

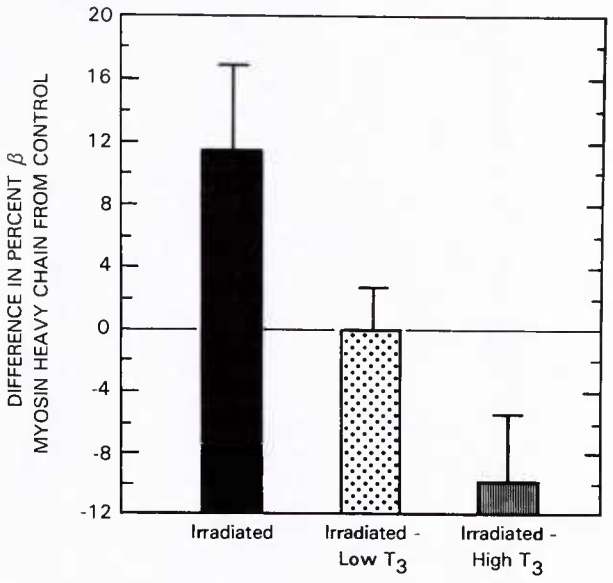

Fig 4. Difference in percent β-myosin heavy chain from age-matched controls for irradiated (10 Gy), irradieted + daily physiological dose (0.3 μg/100 g body weight) of T_3, and irradiated + daily pharmacological dose (3.0 μg/100 g body weight) of T_3 groups following 8 days postirradiation. Values are mean ± SE for four to seven hearts per group. Daily injections of T_3 were started at the time of irradietion. The averege percent β-myosin heavy chain value for the age-matched control wes 14.6 ± 2.9.

The mechanism by which thyroid hormone changes the myosin isozymes appears to occur at the transcriptional level. Several investigators have shown a direct relationship between the mRNA levels and the protein content of the β- and α-myosin heavy chains under conditions of hypo- and hyperthyroidism.[19,20] During the hypothyroid condition, the amounts of β-myosin heavy chain protein and mRNA level are high, while α-myosin heavy chain are very low or nondetectable. During the hyperthyroid state, the opposite events occur. Recently, Umeda et al[10] demonstrated, using transcriptional run-off experiments of heart nuclei, that nascent mRNA levels of the β- and α-myosin heavy chains are regulated by thyroid hormone demonstrating gene transcriptional regulation.

Conditions other than thyroid hormone have been shown to alter the cardiac myosin isozymes. Pressure overload to the heart causes an increase in the synthesis and the amount of β-myosin heavy chain.[7,9,21] Along with this increase in β-myosin heavy chain is an increase in the β-myosin heavy chain mRNA levels.[20,21] However, with these alterations, there was no change in the serum levels of T_4.[9] Others have shown that nutrition can alter the cardiac myosin isozymes without changes in the thyroid hormones. Sheer and Morkin[22] demonstrated an increase in the α-myosin heavy chain with high carbohydrate feeding in hypophysectomized rats. T_3 replacement further increased the percent α-myosin heavy chain demonstrating a synergistic effect. Dillmann[23] showed a similar effect with fructose feeding in thyroidectomized rats. The current study demonstrates that after radiation, V_3 isozyme increases within days and also responds to T_3 injections when serum T_4 is low despite normal serum T_3 levels. This suggests that the myosin isozyme response to thyroid hormone is complex and depends on factors other than circulating T_3 levels. Thus, there may be other factors in addition to thyroid hormones that contribute to the alteration of the cardiac myosin isozymes following whole-body irradiation, although prevention of these changes with T_3 administration strongly suggests thyroid hormone is primarily responsible for the altered myosin isozyme pattern.

The cause for the depression of the serum T_4 level following whole-body irradiation is unknown. Several investigators have also observed this depression of T_4 in rats after whole-body irradiation.[24,25] Gray et al[24] suggested that the radiation-induced T_4 depression is caused, in part, by a change in the clearance rate of T_4 from the blood. Bertok and Nagy[25] postulated that the depressed T_4 is due to enteroendotoxemia developed during the intestinal syndrome of radiation disease. Fasting may also be a cause for a reduced serum T_4 level.[12,26] In our irradiation model, the rats lost weight for the first 5 days, consuming 10% to 20% of normal intake. Unlike fasting alone, which produces a low serum T_3 and TSH,[12,26] the irradiated rats initially had the unexpected combination of an increased TSH and normal serum T_3. Potential explanations for the increased TSH include radiation hypophysitis with release of stored hormone (unlikely, as serum prolactin and luteinizing hormone were unchanged on day 3, data not shown), secretion of a biologically altered form of TSH, or an impaired systemic clearance of TSH. Future experiments will be directed toward understanding the mechanism producing a depressed T_4 and elevated TSH following whole-body irradiation.

Finally, it is interesting that the serum T_3 levels were normal at day 3 and day 6 postirradiation, while the serum T_4 was depressed. This may indicate preservation of the 5′-monodeiodinase despite weight loss. This is supported by one T_3 kinetic study showing that the T_3 production rate began to fall earlier in pair fed than irradiated rats.[24]

In summary, we found a change in the cardiac myosin isozymes following whole-body irradiation. The change toward the β-myosin heavy chain was associated with a depression in the serum T_4 level. Daily injection of T_3 prevented a change in the myosin isozymes. Future experiments will be directed toward the mechanism causing the change in TSH and T_4 levels as well as the functional effect that this may have on the heart.

ACKNOWLEDGMENT

The authors would like to thank Dr Steven Steiffel for the histology studies, Irene Gist and Sandra Smart for technical assistance, and Efigenia Geschke for secretarial assistance.

REFERENCES

1. Hoh JFY, McGrath PA, Hale PT: Electrophoretic analysis of multiple forms of rat cardiac myosin: Effects of hypophysectomy and thyroxine replacement. J Mol Cell Cardiol 10:1053-1076, 1978

2. Martin AF, Pagani ED, Solaro RJ: Thyroxine induced redistribution of isoenzymes of rabbit ventricular myosin. Circ Res 50:117-124, 1982

3. Litten RZ, Martin BJ, Low RB, et al: Structural alterations in contractile proteins from thyrotoxic and pressure-overloaded hypertrophied rabbit hearts, in Alpert NR (ed): Perspectives in Cardiovascular Research: Myocardial Hypertrophy and Failure, vol 7. New York, NY, Raven, 1983, pp 405-425

4. Hoh JFY, Yeoh GPS, Thomas MAW, et al: Structural differences in the heavy chains of rat ventricular myosin isozymes. FEBS Lett 97:330-334, 1979

5. Everett AW, Chizzonite RA, Clark WA, et al: Relationship of changes in molecular forms of myosin heavy chains to endogenous level of thyroid hormone during postnatal growth, in Tarazi RC, Dunbar JB (eds): Perspectives in Cardiovascular Research Cardiac Hypertrophy in Hypertension, vol 8. New York, NY, Raven, 1982, pp 83-92

6. Lompre AA, Mercadier JJ, Wisnewsky C, et al: Species- and age-dependent changes in the relative amounts of cardiac myosin isozymes in mammals. Dev Biol 84:286-290, 1981

7. Mercadier JJ, Lompre AM, Wisnewsky C, et al: Myosin isoenzymic changes in several models of rat cardiac hypertrophy. Circ Res 49:525-532, 1981

8. Litten RZ, Martin BJ, Buchthal RH, et al: Heterogeneity of myosin isozyme content of rabbit. Circ Res 57:406-414, 1985

9. Litten RZ, Martin BJ, Low RB, et al: Altered myosin isozyme patterns from pressure-overloaded and thyrotoxic hypertrophied rabbit heart. Circ Res 50:856-864, 1982

10. Umeda PK, Darling DS, Kennedy JM, et al: Control of myosin heavy chain expression in cardiac hypertrophy. Am J Cardiol 59:49A-55A, 1987

11. Everett AW, Clark WA, Chizzonite RA, et al: Change in synthesis rates of α- and β-myosin heavy chains in rabbit heart after treatment with thyroid hormone. J Biol Chem 258:2421-2425, 1983

12. Dillmann WH, Berry S, Alexander NM: A physiological dose of triiodothyronine normalizes cardiac myosin adenosine triphos-

phatase activity and changes myosin isoenzyme distribution in semistarved rats. Endocrinology 112:2081-2087, 1983

13. Alpert NR, Mulieri LA, Litten RZ: Isoenzyme contribution to economy of contraction and relaxation in normal and hypertrophied hearts, in Jacob R, Gulch RW, Kissling G (eds): Cardiac Adaptation to Hemodynamic Overload, Training, and Stress. Dormstadt, Germany, Steinkopff, 1983, pp 147-157

14. Litten RZ, Walden TL, Gainey GT, et al: Alteration of cardiac myosin isozymes after whole-body irradiation. Br J Radiol 62:189-191, 1989

15. Dillmann WH: Influence of thyroid hormone administration on myosin ATPase activity and myosin isoenzyme distribution in the heart of diabetic rats. Metabolism 31:199-204, 1982

16. Rupp H: Polymorphic myosin as the common determinant of myofibrillar ATPase in different haemodynamic and thyroid states. Basic Res Cardiol 77:34-46, 1982

17. Holubarsch CH, Goulette RP, Litten RZ, et al: The economy of isometric force development, myosin isoenzyme pattern and myofibrillar ATPase activity in normal and hypothyroid rat myocardium. Circ Res 56:76-86, 1985

18. Schwartz K, Lecarpentier Y, Martin JL, et al: Myosin isoenzymatic distribution correlates with speed of myocardial contraction. J Mol Cell Cardiol 13:1071-1075, 1981

19. Everett AW, Sinha AM, Umeda PK, et al: Regulation of myosin synthesis by thyroid hormone: Relative change in the α- and β-myosin heavy chain mRNA levels in rabbit heart. Biochemistry 23:1596-1599, 1984

20. Mahdavi VM, Izumo S, Nadal-Ginard B: Developmental and hormonal regulation of sarcomeric myosin heavy chain gene family. Circ Res 60:804-814, 1987

21. Nagai R, Pritzl N, Low RB, et al: Myosin isozyme synthesis and mRNA levels in pressure-overloaded rabbit hearts. Circ Res 60:692-699, 1987

22. Sheer D, Morkin E: Myosin isoenzyme expression in rat ventricle: Effects of thyroid hormone analogs, catecholamines, glucocorticoids and high carbohydrate diet. J Pharmacol Exp Therap 220:872-879, 1984

23. Dillmann WH: Myosin isoenzyme distribution and Ca^{+2}-activated myosin ATPase activity in the rat heart is influenced by fructose feeding and triiodothyronine. Endocrinology 116:2160-2166, 1985

24. Gray WM, Orr JS, Ratcliffe WA: The effects of whole-body irradiation on the serum levels and kinetics of thyroid hormones in rats. Int J Radiat Biol 37:653-666, 1980

25. Bertok L, Nagy SV: Effect of irradiation on serum T_4 level and response of thyroid gland to exogenous TSH in rats. J Radiat Res 27:225-229, 1986

26. Smallridge RC, Glass AR, Wartofsky L, et al: Investigations into the etiology of elevated serum T_3 levels in protein-malnourished rats. Metabolism 31:538-542, 1982

RADIATION RESEARCH 121, 46–53 (1990)

ARMED FORCES RADIOBIOLOGY RESEARCH INSTITUTE
SCIENTIFIC REPORT
SR90-9

Nonuniform Irradiation of the Canine Intestine

I. Effects

R. M. VIGNEULLE, J. HERRERA,* T. GAGE,* T. J. MACVITTIE, P. TAYLOR,[1] G. ZEMAN,[2] J. B. NOLD,[3] AND A. DUBOIS†

*Armed Forces Radiobiology Research Institute, Bethesda, Maryland 20814-5145; *Walter Reed Army Medical Center, Washington, D.C., and †Uniformed Services University of the Health Sciences, Bethesda, Maryland 20814*

VIGNEULLE, R. M., HERRERA, J., GAGE, T., MACVITTIE, T. J., TAYLOR, P., ZEMAN, G., NOLD, J. B., AND DUBOIS, A. Nonuniform Irradiation of the Canine Intestine. I. Effects. *Radiat. Res.* 121, 46–53 (1990).

To investigate the effects of nonuniform irradiation on the small intestine, we prepared 24 dogs for continent isoperistaltic ileostomies under aseptic surgical conditions and general anesthesia. After a 3-week recovery period, the ileum was catheterized with a fiberoptic endoscope to observe the intestinal mucosa and to harvest mucosal biopsies. The baseline macroscopic and microscopic appearance of the intestinal mucosa was determined. Two weeks later, the ileum was catheterized with a 100-cm soft tube containing 40 groups of three thermoluminescent dosimeters placed at equally spaced intervals, and a dose of either 4.5, 8, 10, 11, or 15 Gy ^{60}Co γ rays was delivered to the right abdomen (nonuniform exposure). This method allowed a direct and precise assessment of the dose received at 40 sites located in the 100-cm intestinal segment. The intestinal mucosa was again evaluated 1, 4, and 6 days after irradiation. All animals exposed to 4.5 and 8 Gy survived, whereas none survived after 11 and 15 Gy. After exposure to 10 Gy, 60% of the animals died within 4–6 days and 40% survived with symptoms associated with both the intestinal and the hematopoietic syndromes. Crypt cell necrosis, blunting of villi, and reduction of the mucosal lining increased between 1 and 4 days after irradiation, and mucosal damage was correlated with intraintestinal dosimetry at Day 6. The granulocyte counts at Day 4 were significantly lower than baseline level in animals that died within 4–6 days but not in survivors. The present model appears to be realistic and clinically relevant, allowing the concurrent study of the intestinal and hematopoietic effects of high-dose nonuniform irradiation similar to that received by patients during radiation therapy as well as by radiation accident victims. © 1990 Academic Press, Inc.

INTRODUCTION

Total-body exposure to ionizing radiation may be lethal in mammals including man (*1*). This lethality results primarily from radiation-induced injury to the radiosensitive stem cells of the hematopoietic and intestinal tissues. Following high-dose irradiation, both rodents and large mammals die from the intestinal syndrome during a 4- to 6-day period that is similar in these species (*1*). However, the dose at which 50% of the animals die on or before Day 6 ($LD_{50/6}$) following total-body irradiation (TBI) is higher for rodents (*1–3*) than for dogs (*4–7*), whereas it is similar in man and in the dog (*8*). Further, TBI of rodents is characterized by uniform dose distribution, whereas TBI of large animals and humans results in a nonuniform distribution of radiation dose due to geometric factors (*9–12*).

In radiation accidents involving humans, the dose distribution in radiosensitive tissues is usually not uniform. Therefore, a realistic model for accidental exposure of man should use a nonuniform rather than a uniform radiation dose. In the past, however, most studies of damage to the small intestine from high-dose radiation used TBI of rodents or bilateral exposure of large mammals. Thus, the response of the intestine of large animals exposed to nonuniform abdominal irradiation has not been adequately studied or described. Specifically, it is unknown whether survival times, hematological effects, and intestinal injury are similar in large animals after a high-dose uniform TBI and after a high-dose nonuniform irradiation of the abdomen. Such data are necessary to determine the appropriate treatment for patients involved in radiation accidents.

In the present study, we used a dog model to determine the effect of nonuniform abdominal irradiation on survival, hematologic parameters, and the time course of intestinal injury. Preparing the animals with ileostomies allowed repeated endoscopic examinations to be carried out. Furthermore, assessment of the macroscopic and microscopic status of the intestinal mucosa was made in the very same animals in which direct intraintestinal dosimetry was performed at the time of irradiation. We also evaluated the

[1] Present address: Department of Radiation Medicine, Georgetown University Hospital, 3800 Reservoir Road N.W., Washington, DC 20007.

[2] Present address: AT&T Bell Laboratories, 600 Mountain Avenue, Murray Hill, NJ 07974-2070.

[3] Present address: Pathology Branch, HHDUSAMRICD, Aberdeen Proving Grounds, MD 21010.

0033-7587/90 $3.00
Copyright © 1990 by Academic Press, Inc.
All rights of reproduction in any form reserved.

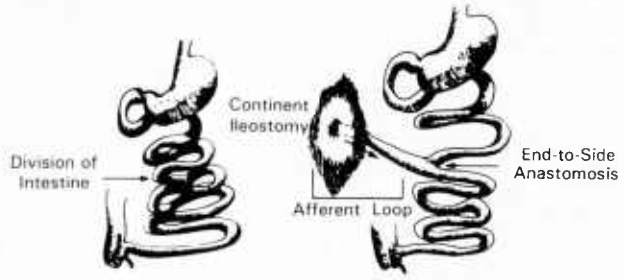

FIG. 1. Schematic representation of the isoperistaltic continent ileostomy surgical preparation used in the dog.

relationship between intraintestinal dosimetry and the corresponding intestinal injury.

MATERIALS AND METHODS

Animals

One- to two-year-old male purpose-bred Hra beagle dogs (12–14 kg) were used in this study. The animals were quarantined on arrival for 14 days and screened for evidence of disease. They were maintained in an AAALAC-accredited facility in runs and provided commercial dog chow and tap water *ad libitum*. The animal holding rooms were maintained at $2 \pm 2°C$ with $50 \pm 10\%$ relative humidity using at least 10 air changes per hour of 100% conditioned fresh air. The dogs were on a 12-h light/dark full spectrum lighting cycle with no twilight.

Surgical Procedure

A continent ileostomy was performed on each of 20 animals 5 weeks before irradiation. In addition, 4 animals were prepared similarly and euthanized as controls for normal morphometry at 5 weeks. Aseptic surgery was performed under general anesthesia. The animals received a subcutaneous (sc) injection of 2.2 mg/kg Rompun (Mobay Corp, Shawnee, KS), and were intubated and anesthetized by inhalation of 4.0% isoflurane in a 67.0% N_2O/33.0% O_2 gas mixture, and were maintained on 1.0% isoflurane in the same gas mixture. A midline laparotomy was performed, and the small intestine was transsected at the midpoint between the pylorus and the ileocecal valve. The distal end of the section was brought through the abdominal wall and sutured to the parietal peritoneum and to the skin to create a continent ileostomy. The proximal end of the transsection was sutured end to side to the distal segment 30 cm from the ileostomy (Fig. 1).

The surgical procedure did not compromise normal gastrointestinal transit; it prevented external loss of succus intestinalis and allowed repeated intubation of the ileum without causing significant side effects. The ileostomy remained patent throughout the studies.

Postoperative, Preirradiation Animal Care

The surgical procedure was well tolerated by all animals and the postoperative period was uneventful. Following recovery from anesthesia, all animals were individually caged and monitored numerous times daily for evidence of pain and discomfort to ensure that their well-being was maintained at the highest standards and that rapid recovery occurred without complications. Normal soft diet was resumed the day following surgery. The few infections that occurred were quickly diagnosed by rising temperature and changes in the complete blood counts. If antibiotic therapy was required, 90 mg/kg Cefotaxime sodium was given intramuscularly (im) as a loading dose, followed by 9 mg/kg im twice daily for 10 consecutive days. The animals used in this study were clinically normal and were fully anesthetized during endoscopic examinations to preclude any possible discomfort.

Endoscopies and Biopsy Frequency

Endoscopies were performed after a 3-week postsurgery recovery period, i.e. 2 weeks before irradiation, to establish baseline values, and at 1, 4, and 6 days after irradiation for histologic studies. Animals were initially given 0.4 mg atropine sulfate im (Elkins-Sinn, Inc., Cherry Hill, NJ), then 2.2 mg/kg Rompun im for sedation preceding anesthesia as described above for the surgical procedure. An Olympus fiberoptic endoscope (GIP3, outside diameter 9.8 mm; Olympus Corp., Lake Success, NY) was then introduced through the ileostomy to permit macroscopic inspection of the intestinal mucosa and the harvesting of mucosal biopsies for histology. A fenestrated biopsy forceps (FB-21, Olympus Corp.) was used to obtain mucosal pinch biopsies which included the muscularis mucosae to ensure that the full depth of the mucosa was obtained and to facilitate proper orientation of the crypts under low magnification light microscopy.

Six biopsies were taken from each mucosal area. Biopsies were placed on a slice of pickled cucumber kept in 70% ethanol and oriented with the villi pointing upward perpendicularly to the flat plane using a fine forceps and a 10× stereomicroscope. This preparation allows processing and sectioning of the tissue plus cucumber slice and permits excellent orientation of intestinal mucosa. Oriented biopsies were fixed for 2 h in Bouin's fixative, transferred to 70% ethanol for dehydration, and embedded in paraffin. Serial 5-μm cross sections were placed on slides and stained with Harris hematoxylin and eosin (H&E).

Biopsies were studied by light microscopy and were graded blindly by JBN for radiation damage to the intestinal mucosa using the following grading score: (0) no damage (Fig. 2A); (1) normal villus epithelium and cellular necrosis restricted to crypt epithelium (Fig. 2B); (2) blunting of some villi that contain atypical epithelial cells and some collapsed crypts with increased necrosis; and (3) blunting and denudation of most villi, plus edema, ulceration of surface epithelium, and collapse of many crypts (Fig. 2C).

Morphometry

Computer-assisted morphometric measurements (Bioquant System IV; R&M Biometrics, Inc., Nashville, TN, 1985) were made on tissues obtained from eight euthanized animals (four unirradiated controls and four having received 10 Gy abdominal irradiation). Intestinal specimens were taken from the ileal sites where the radiation dose had been determined by intraintestinal dosimetry. Tissues were fixed in 10% buffered formalin. Transverse sections were embedded in paraffin. Serial 5-μm sections of the paraffin-embedded tissue spaced 100 μm apart were placed on glass slides and stained with H&E. At least five slides of the tissues of each of three or more animals were analyzed. Only crypts containing healthy looking cells were counted. The number of crypts per millimeter of circumference was scored. Crypt depth in millimeters was measured from the base of the villus to the muscularis mucosa. The base of the villus was determined by comparing several adjacent villi and drawing a line through the estimated bases of several villi. Villus height and villus-crypt length were measured in millimeters. Cell numbers were analyzed for the combined length from the bottom of the crypt to the top of the villus, because the division between villus and crypt is not distinct.

Irradiation

The abdomen of each surgically prepared animal was irradiated with 4.5 ($N = 2$), 8 ($N = 4$), 10 ($N = 10$), 11 ($N = 4$), or 15 ($N = 4$) Gy nominal midline doses, as described in detail in the companion paper by Zeman *et al.* (*13*), and using a 24 × 40-cm field of exposure. In brief, the right side of the animal was facing a 63,200 Ci ^{60}Co γ radiation source placed 118 cm from the skin. The four lower ribs were included in the field, while the vertebrae and the remainder of the animal were shielded with 5 cm of lead.

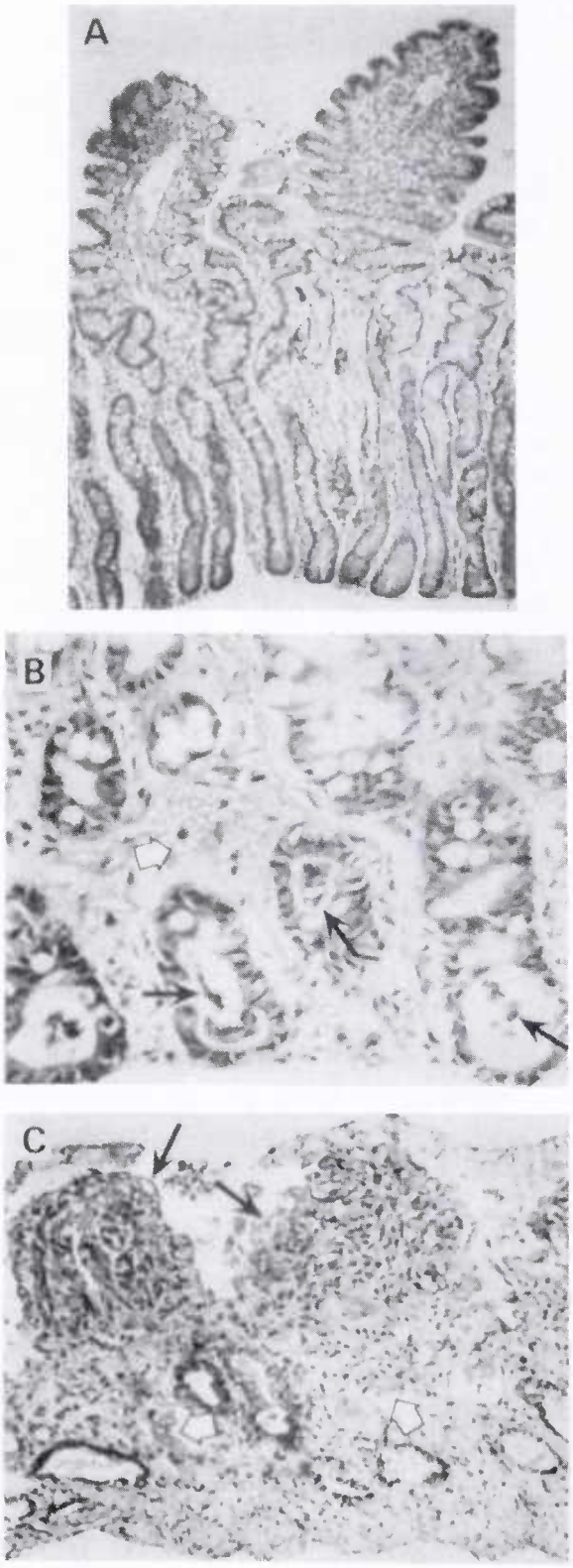

FIG. 2. Histologic appearance of intestinal biopsies after H & E preparation. (A) Control mucosa (grade 0) with elongated villi and deep crypts lined by cuboidal to tall columnar epithelium, 150×. (B) Day 1 mucosa after 11.2 Gy (grade 1), 850×. Note cellular necrosis involving crypt epithelium (solid arrows) and the edema and hemorrhage in the lamina propria (open arrows). (C) Day 4 mucosa after 7.2 Gy (grade 3), 360×. The villi are severely blunted and lined by atypical epithelial cells (solid arrows). Numerous areas of ulceration are present. Many crypts are collapsed while others are hypocellular and lined by hypertrophied epithelial cells (open arrows). A necrotic cellular exudate overlies the mucosa and fills some crypts.

The radiation dose was delivered to the midline at an average dose rate of 3.75 Gy/min during 4 min or less. The radiation dose to the shielded portion of the spine and ribs that were within 5 cm of the edge of the open field was 7 to 10% of the radiation dose at the center of the exposure field. Other shielded body areas including the head and the remainder of the bone marrow received radiation doses less than 7%. Thermoluminescent dosimeters were used to determine radiation doses received at 40 specific locations of the intubated ileum as described in detail in the companion paper (*13*).

During irradiation, the animals were immobilized in a standing position in a Plexiglas box using Plexiglas rods. The box was constructed of pieces of 6-mm-thick Plexiglas fitted together; the lateral pieces were held in place by Plexiglas rods and aluminum retaining rings. The animal's head was left outside the box and was supported under the chin but not immobilized.

Animal Care Postirradiation

After irradiation, the animals were housed in individual cages and received 500 ml of sterile Ringer's lactate solution sc (Travenol Laboratories, Inc., Deerfield, IL) and 4 mg/kg gentamycin sulfate im (Lyphomed, Inc., Melrose Park, IL) daily for antibiotic prophylaxis for 14 consecutive days. They were evaluated daily for appetite, hydration, health status, and presence of diarrhea. A complete blood count was performed 5 days a week. If an animal's health deteriorated beyond therapy, euthanasia was performed with 60 mg/kg T-61 Euthanasia Solution given intravenously (Taylor Pharmacal Co., Decatur, IL).

Statistical Analysis and Curve Fitting

Regression analysis and χ^2 analysis (2 by 2 contingency table) were performed using standard techniques. Curve fitting was performed using a VAX computer (Digital Equipment Corp., Landover, MD) and RS/1 software (BBN Software Products Corp., Cambridge, MA) for a Weibull power exponential (*14*).

RESULTS

Survival

Following surgery, oral intake and intestinal transit were not modified, weights were maintained ±2 kg, and none of the animals died during the preirradiation period. In contrast, following irradiation, these animals did experience vomiting and diarrhea which were not quantitated. The dose–response curve for the effects of abdominal irradiation on survival is shown in Fig. 3. The Weibull power exponential fit of these data provided an $LD_{50/6}$ of 9.7 ± 1 Gy. All animals exposed to a midline dose greater than 10 Gy died or were killed before Day 6 (11 Gy, 0/4; 15 Gy, 0/4), while all animals exposed to 4.5–8 Gy survived (6/6). In the group of animals exposed to 10 Gy, 40% of the animals survived 6 days or longer (4/10), and 30% survived 30 days (3/20; one died at 22 days). Therefore, the animals that received 10 Gy were divided into those that died early, before Day

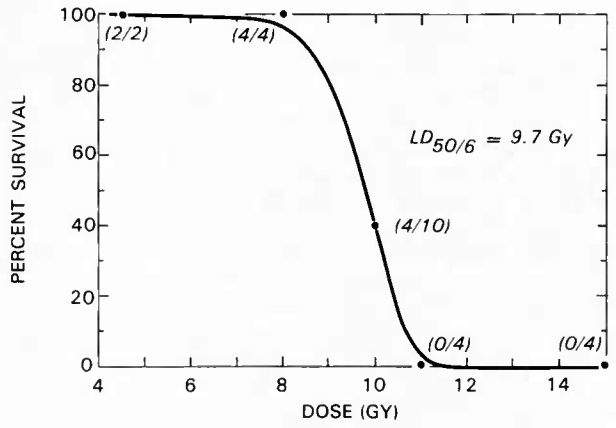

FIG. 3. Weibull relation between nominal midline dose of abdominal irradiation and survival in dogs.

6, and those that survived beyond 6 days. The results of intraileal dosimetry were not different among these two groups (Table I).

Peripheral Hematology

The peripheral blood granulocyte count was significantly decreased at Day 4 in animals that received 10 Gy compared to baseline levels ($P < 0.05$; Table II), but values were significantly higher in survivors than in nonsurvivors ($P < 0.05$). In contrast, the peripheral blood lymphocyte counts at Day 4 were similar in both groups but significantly lower than baseline unirradiated values ($P < 0.05$). Platelets were not significantly modified at Day 4 in either group. A platelet count nadir of 106,000 ± 10,503 (30.6% of preirradiation value) was observed at Day 11 in the animals that survived beyond 6 days. Red blood cell counts and hematocrit values were significantly ($P < 0.05$) elevated only in animals that died by Day 6.

Endoscopy

Before irradiation, the surface of the intestinal mucosa had a glistening appearance and there was little or no granularity or edema (Fig. 4A). Slight edema and granularity were present at Day 1. At Day 4, edema, granularity, submucosal hemorrhage, submucosal bleeding, and ulcerations were observed, and the tissue was friable; the extent of the damage appeared to depend on the radiation dose. This damage was observed consistently and was estimated qualitatively. In areas of the intestinal mucosa exposed to less than 8 Gy, edema, granularity, and erythema were slight to mild and the tissues were somewhat friable; submucosal hemorrhage was observed only occasionally. At doses between 8 and 10 Gy, the mucosa was friable, edema, granularity, and erythema were moderate to severe, bleeding and submucosal hemorrhage were observed more frequently, and ulceration was common. Above 10 Gy, bleeding and submucosal hemorrhage prevented observation of the mucosa (Fig. 4B).

Histopathology of Mucosal Biopsies

The intestinal mucosa was characterized during the postsurgery preirradiation period by elongated villi and by deep crypts lined with cuboidal to tall columnar epithelium

TABLE I
Intraileal Dosimetry and Corresponding Duration of Survival after a Nominal 10-Gy Midline Abdominal Exposure

Animal no.	Mean dose ± SEM[a] (Gy)	Median	Range	Geometric mean	Survival (No. of days)
		Survival < 6 days			
1.	9.05 ± 0.33	9.42	5.94–11.70	8.86	4
2.	8.81 ± 0.47	7.93	3.36–12.46	8.40	4
3.	8.11 ± 0.48	8.16	2.65–12.39	7.58	4
4.	9.16 ± 0.27	9.14	6.64–12.27	9.05	4
5.	7.73 ± 0.18	7.68	6.19–9.68	7.66	5
6.	9.09 ± 0.33	9.42	4.43–12.23	8.88	4
Mean ± SEM	8.65 ± 0.36	8.63		8.40	
		Survival 22–30 days			
1.	8.04 ± 0.31	7.90	5.36–12.38	7.85	22
2.	9.37 ± 0.44	9.78	4.97–12.70	9.01	30
3.	8.96 ± 0.26	8.44	6.81–12.54	8.85	30
4.	10.02 ± 0.29	10.33	7.87–11.92	9.88	30
Mean ± SEM	9.09 ± 0.33	9.11		8.89	

[a] Mean intraintestinal dose of 30–32 ileostomy locations.

TABLE II
Peripheral Blood Parameters 4 Days after 10 Gy Abdominal Irradiation

Parameter	Preirradiation	Animals dying by day 6	Animals surviving 22–30 days
WBC	11,850 ± 360	2,216 ± 559*	5,450 ± 1,292*,**
RBC	6,120 ± 140	7,771 ± 623*	5,765 ± 208**
Total granulocytes	8,520 ± 376	1,653 ± 552*	4,525 ± 1,296*,**
Total lymphocytes	2,933 ± 162	522 ± 102*	499 ± 130*
Hematocrit %	40.4 ± 0.89	51.6 ± 4.0*	37.8 ± 1.6
Platelets	364,000 ± 19,000	472,500 ± 79,500	488,500 ± 27,600

* $P < 0.05$ compared to preirradiation values.
** $P < 0.05$ compared to early death group.

(Grade 0; Fig. 2A). One day after irradiation, there was mild damage only in areas exposed to more than 10 Gy; this damage was characterized by cellular necrosis in the crypts (Grade 1; Fig. 2B, solid arrows) and hemorrhage and edema in the lamina propria (open arrow); the villi appeared normal (not shown). Severe mucosal damage appeared at 4 days after all doses of radiation (Grade 3; Fig. 2C). The villi were blunted and lined by atypical epithelial cells (solid arrows). Numerous areas of ulceration were present. Many crypts were collapsed while others had fewer cells and were lined by atypical epithelial cells (open arrows). A necrotic cellular exudate overlaid the mucosa and filled some crypts.

Before irradiation, histology was comparable in all groups (Table III). One day after irradiation, the fraction of biopsies with a histology grading score > 0 was significantly increased after abdominal exposure to a midline dose of 10 Gy but not after 4.5–8 Gy. On Day 4, all groups had increased histological damage, but there was no statistically significant difference between animals dying before Day 6 and those surviving beyond Day 6 in the 10-Gy irradiated group. On Day 6, in animals exposed to 4.5–8 Gy, there was no longer histological evidence of damage, whereas animals exposed to 10 Gy continued to display significant damage whether they survived beyond 6 days or not ($P < 0.01$ vs baseline). Therefore, exposure to higher doses of radiation consistently produced significantly more damage at Day 6 ($P < 0.01$ vs 4.5–8 Gy animals).

There was no significant correlation between the intraintestinal dose and the corresponding histology grading score of biopsies obtained at Days 1 and 4 ($R = 0.004$ and 0.029, respectively). In contrast, the histology grading score of Day 6 biopsies was significantly correlated with the corresponding intraintestinal dose ($R = 0.89$; $P < 0.01$; Fig. 5).

Morphometry of the Ileal Mucosa

Four days after abdominal exposure to 10 Gy, crypt number and villus height were the only parameters that

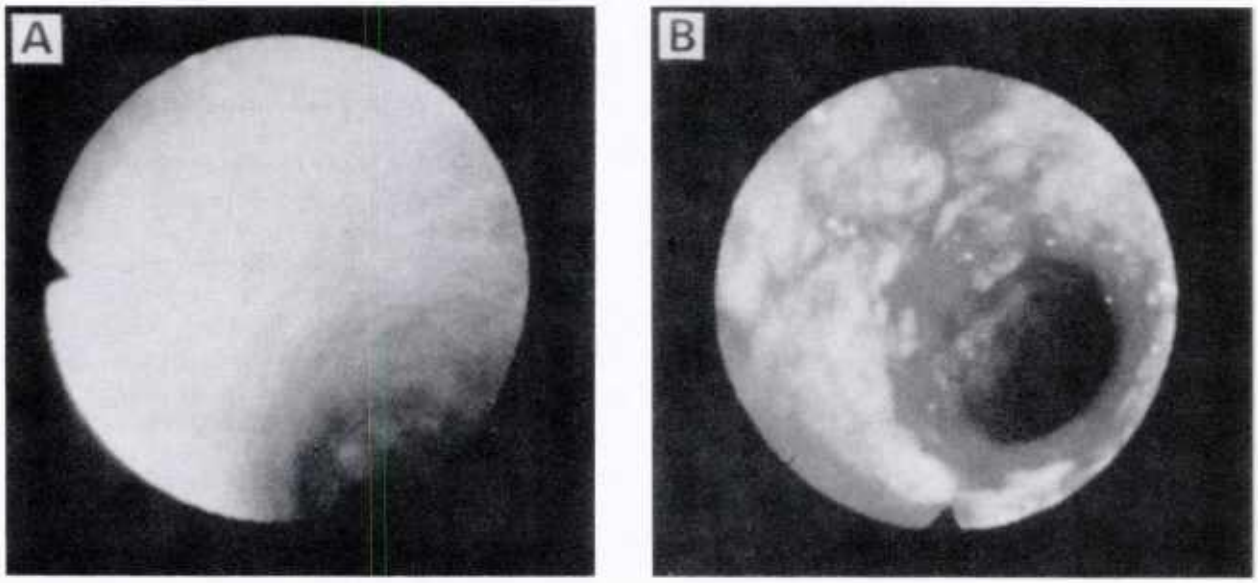

FIG. 4. Endoscopic appearance of the intestinal mucosa in the control nonirradiated state (A) and after exposure to 10 Gy at Day 4 (B). Note bleeding and submucosal hemorrhage in intestinal mucosa exposed to 10 Gy.

TABLE III
Fractions of Ileal Biopsies Obtained at Endoscopy That Had a Histology Grading Score Greater than Zero

	4.4–8.0 Gy	(10 Gy)		
	Animals surviving 30 days[a]	Animals dying by day 6	Animals surviving 22–30 days	Total[b]
Preirradiation	2/9	1/7	1/14	2/21
Day 1	6/10	4/4**	7/8**	11/12**
Day 4	7/9*	6/6**	16/16**	24/24**
Day 6	2/10	4/4**,****	2/2**,***	6/6**,****

[a] All animals survived to 30 days following 4.5–8.0 Gy irradiation.
[b] Sum of the animals that survived 22 to 30 days + animals that survived to 6 days.
* $P < 0.05$ compared to its own baseline.
** $P < 0.01$ compared to its own baseline.
*** $P < 0.05$ compared to 4.5–8.0 Gy group.
**** $P < 0.01$ compared to 4.5–8.0 Gy group.

were significantly reduced in animals dying by Day 6 compared to unirradiated controls ($P < 0.05$; Table IV). The villus height was decreased to 58% of the control value and crypt depth to 84%. The number of crypts per millimeter of intestine and the number of cells from crypt to villus were reduced to 78 and 76% of control values, respectively. No morphometry was performed at Day 4 in animals surviving beyond Day 6.

TABLE IV
Mucosal Radiation Injury Determined from Morphometric Measurements of Control Unirradiated Dogs and Dogs Given 10 Gy Abdominal Irradiation at Day 4

Parameter	Control	Irradiated
Crypts per mm	15.9 ± 1.0	14.3 ± 0.4
	21.7 ± 0.4	17.4 ± 0.7
	23.4 ± 0.4	17.4 ± 0.5
	22.9 ± 0.5	13.9 ± 0.4
Mean ± SEM	20.9 ± 1.7	15.8 ± 1.0*
Villus height (mm)	0.80 ± 0.03	0.46 ± 0.03
	0.73 ± 0.01	0.41 ± 0.01
	0.82 ± 0.02	0.38 ± 0.01
	0.82 ± 0.01	0.33 ± 0.01
Mean ± SEM	0.79 ± 0.02	0.40 ± 0.03*
Crypt depth (mm)	0.37 ± 0.03	0.37 ± 0.02
	0.31 ± 0.01	0.34 ± 0.01
	0.41 ± 0.02	0.31 ± 0.01
	0.46 ± 0.02	0.34 ± 0.02
Mean ± SEM	0.39 ± 0.03	0.34 ± 0.01
Cells/mm crypt-villus	241.6 ± 12.8	160.9 ± 2.7
	258.9 ± 4.1	180.7 ± 6.0
	234.7 ± 5.1	211.1 ± 3.9
	189.0 ± 3.6	196.7 ± 8.3
Mean ± SEM	231.1 ± 14.9	187.4 ± 10.8

Note. Values are means ± SEM.
* $P < 0.05$ compared to nonirradiated control values.

DISCUSSION

This dog ileostomy model made it possible to observe and sample the small intestinal mucosa before and after unilateral abdominal irradiation and allowed each animal to serve as its own control. By using this model for high-dose-rate nonuniform irradiation, it was possible to study intestinal radiation damage incurred under conditions similar to those likely to occur in radiation accidents.

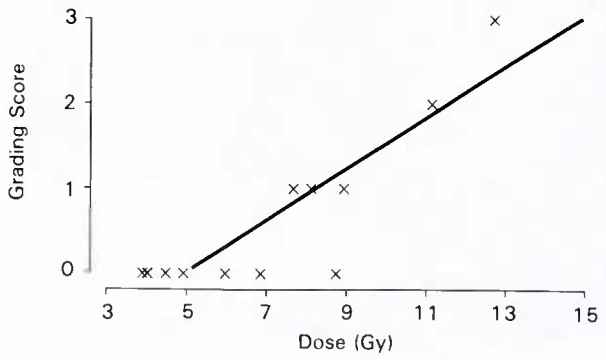

FIG. 5. Relation between histology grading scores and intraintestinal dose at Day 6 (linear regression $R = 0.89$).

By using the dosimetry method described in the companion paper (*13*), we found that the dose to specific sites in the small intestine cannot be predicted precisely based on midline dosimetry (see Table I). Therefore, selecting the midline dose calculated from phantom studies, entry-side dosimetry, or exit-side dosimetry does not accurately reflect the dose received by the mucosa in different segments of the intestine. This is especially important because the extent of the intestinal lesions appears to depend on the dose received by the mucosa at a specific site (Fig. 5). Thus, we observed that the macroscopic and microscopic appearance of the ileal mucosa 6 days after high-dose nonuniform irradiation was directly correlated with the corresponding intraintestinal dosimetry as measured *in situ* using thermoluminescent dosimeters placed in the ileum at the time of irradiation. In contrast, there was no significant correlation between intraintestinal dose and histologic damage at Days 1 and 4. The time course of radiation injury (Table III) appeared to be similar to that observed after uniform abdominal irradiation in a serial autopsy series, in that the damage peaked 4 days after 4.5- and 8-Gy nonuniform irradiation (*7*). However, similar damage was still present at Day 6 in animals exposed to 10 Gy (Table III).

The radiation dose rate is expected to influence the response when the abdomen of large animals is irradiated. However, the $LD_{50/6}$ observed in the present study when 9.7 Gy was delivered at a high dose rate (3.7 Gy/min) was only slightly greater than in a previous study (9.3 Gy) when the exposure was to 250 kVp X rays with a dose rate of 0.6 Gy/min (*7*). Whereas the $LD_{50/6}$ of TBI and abdominal irradiation are reasonably comparable for uniform low-dose-rate X-ray exposures (8.5 Gy vs 9.3 Gy; Refs. (*6, 7*)), these values are lower than found in our study of nonuniform abdominal irradiation with ^{60}Co γ rays. Taken together, these data suggest that death from intestinal damage in large animals depends quantitatively on the radiation dose more than on the dose rate, and that there is some influence of the nonuniformity of the exposure.

The $24 \times 40\text{-cm}^2$ rectangular radiation field used in the present study included the bone marrow of the lower four ribs, whereas the bone marrow of the associated vertebrae and the remainder of the body was shielded. The granulocyte counts were significantly reduced at Day 4 compared to baseline control values, but this reduction was greater in the animals that died before Day 6 than in those that survived. In fact, the difference may even be underestimated because of the hemoconcentration demonstrated in animals dying by Day 6 by the significantly greater RBC count at Day 4 (Table II). Thus, although the exposure of the bone marrow of the two groups of animals was similar, the granulocyte levels of the surviving dogs were significantly higher than those of the dogs that died before Day 6. This finding was not anticipated, nor can it be explained by the shielding characteristics. In addition, radiation doses to the bone marrow of the ribs, spine, and long bones outside the radiation field were low (<10% of nominal midline dose) as indicated by dosimetry behind the lead shield. Therefore, the lower granulocyte levels in the animals dying by Day 6 may be explained either by differences in the radiation response among the nonuniformly irradiated animals which received an $LD_{50/6}$ abdominal radiation dose or by other factors which are unknown at present. However, the correlation between the granulocyte level and survival at Day 4 suggests that the level of granulocytes is a good biological indicator of the outcome of exposure to these doses in dogs.

Our endoscopic, histologic, and morphometric observations demonstrate major radiation-induced changes characterized by bleeding and submucosal hemorrhage in the small intestine of the dog at 4 days after abdominal irradiation. A midline nonuniform abdominal dose of 9.38 Gy at a lower dose rate produced similar severe damage to the mucosa of the small intestine as well as decreased intestinal motility at Day 4 (*7*). At this dose, villus blunting probably resulted in a reduced absorptive surface area that may be responsible in part for intestinal lethality (*1, 7, 8, 12*). Therefore, the lesions observed in biopsies appear to reflect the dose received, although our data suggest that the lesions cannot be used to predict survival. The correlation between the intraintestinal dose and the endoscopic and histopathologic observations demonstrates that the dog ileostomy model allows the study of radiation-induced intestinal damage following a nonuniform high-dose irradiation. The morphometry was not performed for the surviving group of animals for technical reasons. However, the present histopathologic observations are consistent with previous reports that have described the changes in the intestinal mucosa resulting from high-dose irradiation (*1–3, 7, 9–11*). In addition, our report documents these changes in a quantitative manner, while providing repeated measurements in the same animals during the early postirradiation period. Finally, we demonstrated a relationship between, on one hand, the lesions of the ileal mucosa and, on the other hand, both the dose received by these mucosal sites and the animals survival.

This experimental model has provided information which was not previously available for nonuniform irradiations. In the past, specimens obtained at necropsy in different groups of animals were used to determine the effects of nonuniform irradiation on the macroscopic and microscopic appearance of the ileal mucosa at various times after irradiation (*7*). In addition, the absorbed dose to the intestines was reported as a midline tissue dose that had been previously determined with thermoluminescent dosimetry using an irradiated phantom (*7*). In contrast, the present model allowed direct measurements of intraintestinal dose as well as a study of the time course of intestinal injury in the same animals. Furthermore, the macroscopic and microscopic appearances of the ileal mucosa after nonuniform abdominal irradiation were related to the direct intraintestinal dose received by the precise segments of the ileal mucosa which were examined. However, as shown in Table I, there was no significant difference between survivors and nonsurvivors when using either the mean, the median, the range, or the geometric mean of the ileal dosimetry; this suggests that the effects of doses ranging from 8 to 10 Gy cannot be distinguished on the basis of survival. Although this finding is a negative one, it has important implications for the treatment of accidental irradiation.

Future studies using this model should provide information on both the acute sensitivity of the small intestine to radiation and the mechanism involved in early radiation-induced mucosal abnormalities. In addition, this model provides a unique opportunity for testing the mechanism of action of new therapies on the improvement of intestinal function and survival during the first month after accidental or therapeutic nonuniform irradiation (*15–17*).

ACKNOWLEDGMENTS

We thank Mrs. Diane Kreft, Mr. Michael White, Ms. Teresa Pelkey, Mrs. Lillie Heman-Ackah, and Mr. Richard T. Brandenburg for their ex-

cellent technical assistance. Also, we thank Mr. William E. Jackson for assistance with the statistical analysis. This research was supported by the Armed Forces Radiobiology Research Institute, Defense Nuclear Agency, under work units 107 and 131. The opinions and assertions contained herein are those of the authors; no endorsement by the Defense Nuclear Agency has been given or should be inferred. The experiments reported herein were conducted according to the principles set forth in the "Guide for the Care and Use of Laboratory Animals," Institute of Animal Resources, National Research Council, DHEW Publication No. (NIH) 78-2.

RECEIVED: March 27, 1989; ACCEPTED: August 8, 1989

REFERENCES

1. V. P. BOND, T. M. FLIEDNER, and J. O. ARCHAMBEAU, *Mammalian Radiation Lethality. A Disturbance in Cellular Kinetics.* Academic Press, New York, 1965.
2. H. QUASTLER, Studies on roentgen death in mice. I. Survival time and dosage. *Am. J. Roentgenol.* **54,** 449–456 (1945).
3. H. QUASTLER, E. F. LANZL, M. E. KELLER, and J. W. OSBORNE, Acute intestinal death. Studies on roentgen death in mice III. *Am. J. Physiol.* **164,** 546–556 (1951).
4. W. P. NORRIS, T. E. FRITZ, C. E. REHFELD, and C. M. POOLE, The response of the beagle dog to cobalt-60 gamma radiation: Determination of the $LD_{50(30)}$ and description of associated changes. *Radiat. Res.* **35,** 681–708 (1968).
5. H. M. VRIESENDORP, P. HEIDT, and C. ZURCHER, Gastrointestinal decontamination of dogs treated with total body irradiation and bone marrow transplantation. *Exp. Hematol.* **9,** 904–916 (1981).
6. H. M. VRIESENDORP, W. M. KLAPWYK, P. J. HEIDT, B. HOGEWEG, C. ZURCHER, and D. W. VAN BEKKUM, Factors controlling the engraftment of transplanted dog bone marrow cells. *Tissue Antigens* **20,** 63–80 (1982).
7. R. W. SUMMERS, A. W. FLATT, M. J. PRIHODA, and F. A. MITROS, Effect of irradiation on morphology and motility of canine small intestine. *Dig. Dis. Sci.* **32,** 1402–1410 (1987).
8. H. M. VRIESENDORP and D. W. VAN BEKKUM, Susceptibility of total body irradiation. In *Response Of Different Species To Total Body Irradiation* (J. J. Broerse and T. J. MacVittie, Eds.), pp. 43–57. Nijhoff, Dordrecht, The Netherlands, 1984.
9. V. P. BOND, M. N. SWIFT, A. C. ALLEN, and M. C. FISHLER, Sensitivity of abdomen of rat to x-irradiation. *Am. J. Physiol.* **164,** 323–330 (1956).
10. R. A. CONARD, E. P. CRONKITE, G. BRECHER, and C. P. A. STROME, Experimental therapy of the gastrointestinal syndrome produced by lethal doses of ionizing radiation. *J. App. Physiol.* **9,** 227–233 (1956).
11. R. A. CONARD, Some effects of ionizing radiation on the physiology of the gastrointestinal tract: A review. *Radiat. Res.* **5,** 167–188 (1956).
12. M. N. SWIFT and S. T. TAKETA, Modification of acute intestinal radiation syndrome through shielding. *Am. J. Physiol.* **185,** 85–91 (1956).
13. G. H. ZEMAN, T. H. MOHAUPT, P. L. TAYLOR, T. J. MACVITTIE, A. DUBOIS, and R. M. VIGNEULLE, Nonuniform irradiation of the canine intestine. II. Dosimetry. *Radiat. Res.* **121,** 54–62 (1990).
14. E. J. GUMBELL, *Statistics of Extremes.* Columbia Univ. Press, New York, 1958.
15. K. F. BAVERSTOCK and P. J. N. D. ASH. A review of radiation accidents involving whole body exposure and the relevance to the LD 50/60 for man. *Br. J. Radiol.* **56,** 837–849 (1983).
16. A. DUBOIS and R. A. WALKER. Prospects for management of gastrointestinal injury associated with the acute radiation syndrome. *Gastroenterology* **95,** 500–507 (1988).
17. H. M. VRIESENDORP and T. J. MACVITTIE. Animal models for radiation accidents. In *Controversies in Bone Marrow Transplantation* (R. P. Gale and R. Champlin, Eds.), pp. 659–670. A. R. Liss, New York, 1989.

RADIATION RESEARCH 121, 54–62 (1990)

ARMED FORCES RADIOBIOLOGY RESEARCH INSTITUTE
SCIENTIFIC REPORT
SR90-10

Nonuniform Irradiation of the Canine Intestine

II. Dosimetry

G. H. ZEMAN,[1] T. H. MOHAUPT,[2] P. L. TAYLOR,[3] T. J. MACVITTIE, A. DUBOIS,* AND R. M. VIGNEULLE

*Armed Forces Radiobiology Research Institute, and *Uniformed Services University of Health Sciences, Bethesda, Maryland 20814-5145*

ZEMAN, G. H., MOHAUPT, T. H., TAYLOR, P. L., MACVITTIE, T. J., DUBOIS, A., AND VIGNEULLE, R. M. Nonuniform Irradiation of the Canine Intestine. II. Dosimetry. *Radiat. Res.* 121, 54–62 (1990).

An experimental model has been developed for quantitative studies of radiobiological damage to the canine small intestine following partial-body nonuniform irradiation. Animals were irradiated with ^{60}Co γ rays to simulate the nonuniform irradiation which do occur in victims of radiation accidents. The model used a short source-to-surface distance for unilateral irradiations to produce a dose gradient of a factor of two laterally across the canine intestinal region. The remainder of the animal's body was shielded to prevent lethal damage to the bone marrow. *In situ* dosimetry measurements were made using thermoluminescent dosimeters to determine the radiation dose delivered as a function of position along a segment of the small intestine. This system made it possible to correlate the radiation dose delivered at a specific point along the small intestine with the macroscopic and microscopic appearance of the intestinal mucosa at that point, as determined by direct observation and biopsy using a fiberoptic endoscope. A key feature of this model is that dosimetry data for multiple sites, which receive a graded range of radiation doses, can be correlated with biological measurements to obtain a dose–response curve. This model is being used to evaluate the efficacy of new therapeutic procedures to improve survival following nonuniform irradiation. © 1990 Academic Press, Inc.

INTRODUCTION

Central to the prediction of the outcome of highly nonuniform or partial-body irradiation is accurate assessment of the injury after either accidental or therapeutic exposures. In the documented accidents involving fatal irradiation of humans, most victims received highly nonuniform doses (*1*). Nevertheless, current knowledge of the biomedical effects of nuclear radiation is based largely on studies using uniform exposures. Standards of dose uniformity for radiobiology research, defined by the International Commission on Radiation Units and Measurements (*2*), specify no more than 10% dose variation across an animal for "uniform" irradiation and no more than 30% variation for "moderately uniform." The 10% uniformity criterion is readily achieved in most small animal studies. The moderately uniform criterion is possible with many larger animal irradiations if multilateral exposure is used or if the experimental subject is rotated.

This paper describes our efforts to develop a method to determine radiation dose deposition along the intestinal tract more accurately following nonuniform localized irradiation. One critical component of the experiment is the use of a large animal model (canine) so that a highly nonuniform dose will be distributed across the GI tract; this is essential if analogy is to be made to human radiation exposures. A second component of the experiment is the use of *in situ* dosimetry which, along with endoscopy and tissue biopsies of the small intestine, makes site-specific studies of radiation damage along the length of the intact intestine possible.

MATERIALS AND METHODS

Inserting a dosimetry tube or an endoscope into the small intestine, either through the nasogastric route or through the rectum, poses severe logistical complications. To sidestep these complications, a continent ileostomy was created to provide a direct access to the ileum that does not interfere with transit through the small intestine. This procedure utilizes a modified "Roux-en-Y" surgical preparation which is described in detail in the companion paper (*4*).

In vivo dosimetry was done using Harshaw (Solon, Ohio) TLD-100 lithium fluoride thermoluminescent dosimeter chips (TLDs) encased in gelatin capsules with tissue-equivalent plastic filling the gaps. Three TLDs were loaded into each capsule to provide replicate measurements. Two separate dosimetry tubes were developed (Fig. 1). The first contained 30 TLD capsules loaded in a 90-cm length of Tygon tubing. By making dose measurements every 3 cm, it was assured that no two adjacent measurements would differ by more than 20% and no sizable interpolations would be required. Later, a second 90-cm tube was loaded with only 15 TLD capsules because our experience with the first tube indicated that dose measurements every 5 to 6 cm were adequate to define the dose profile along the length of the intestine.

Nylon spheres and a capsule of lead (Pb) beads were positioned between adjacent dosimetry capsules in each Tygon dosimetry tube. The capsule

[1] Present address: AT&T Bell Laboratories, 600 Mountain Avenue, Murray Hill, NJ 07974-2070.

[2] Present address: Great Lakes Naval Hospital, Great Lakes, IL 60088.

[3] Present address: Department of Radiation Medicine, Georgetown University Hospital, 3800 Reservoir Road N.W., Washington, DC 20007.

0033-7587/90 $3.00
Copyright © 1990 by Academic Press, Inc.
All rights of reproduction in any form reserved.

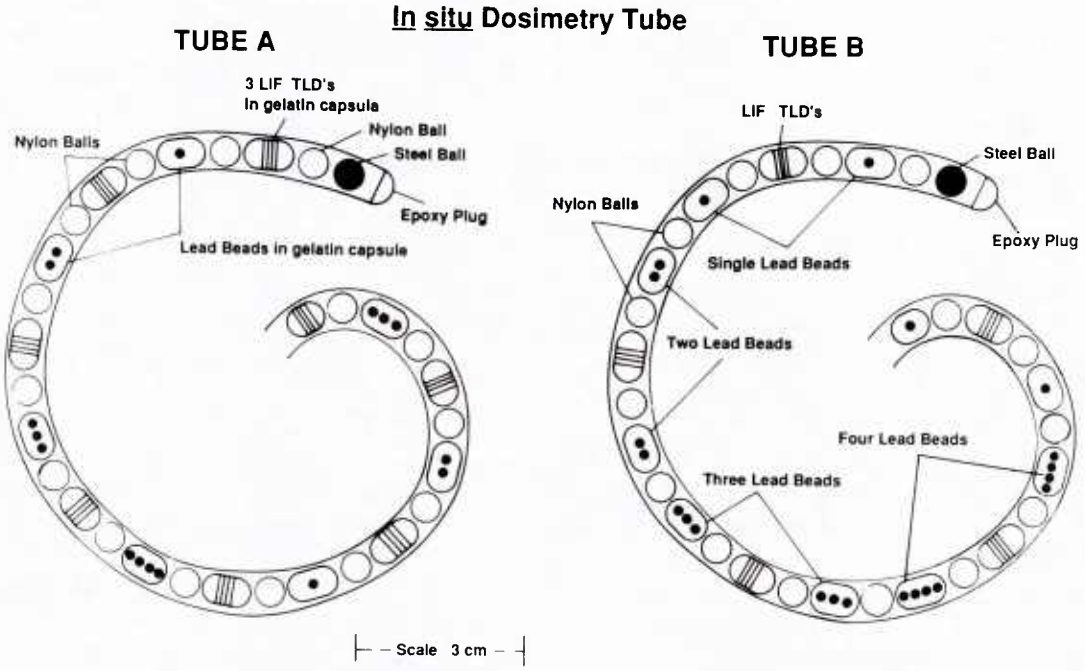

FIG. 1. Dosimetry tubes used for *in vivo* TLD measurements. Tube A was used for high resolution measurements, with a TLD group positioned every 3 cm. In tube B the distance between TLD groups was 6 cm. The distinct lead marker sequences in each tube facilitated TLD localizations on radiographs.

with Pb beads had one, two, three, or four beads epoxied in place to prevent movement. The capsules were spaced sequentially in the Tygon tube to identify locations on orthogonal radiographs taken before and, in some cases, after irradiation. A Pb solder marker was also used to locate the exit end of the tube on the radiographs. The nylon spheres were used as spacers to separate the TLD capsules from those containing Pb beads, thereby preventing any local shielding effects.

The leading end of each dosimetry tube was identified by a unique steel bead. To facilitate passage of the tube through the intestinal lumen, the leading end was sealed with epoxy to a smooth rounded finish and lubricated. The dosimetry tube was flexible and easily followed the tortuous path of the small intestine.

After exposure the TLDs were read on either a Harshaw Automatic Reader Model 2000D or a Harshaw TL Analyzer Model 2080. Each batch of TLDs was calibrated with a Theratron-80 ^{60}Co beam with exposure rate calibration traceable to the National Institute of Standards and Technology. Individual TLDs within each batch varied in sensitivity by a standard deviation of the mean response of the TLDs of approximately 4%. For each batch, five sets of four TLDs were irradiated to develop a calibration function (Fig. 2) to correlate TLD response to absorbed dose.

After the dosimetry tube was inserted into the canine's ileum and secured to prevent slippage, the point on the tube where it exited the stoma was marked for reference. The animal was placed in an acrylic restraint box with sides 6 mm thick. The locations of the lead beads were documented on orthogonal radiographs made using a diagnostic X-ray machine (see Results). The course of the dosimetry tube within the animal was determined from the sequence of Pb beads on the resulting films.

Canines were unilaterally irradiated in the Armed Forces Radiobiology Research Institute (AFRRI) Whole Body ^{60}Co Irradiation Facility (Fig. 3). The distance between the ^{60}Co source and the canine midline was 118 cm. At this distance a dose gradient of a factor of two across the animal was expected on the basis of computer-generated isodose curves for a cylindrical water phantom (Fig. 4). Preirradiation dosimetry measurements were made each day using AFRRI 50 cm^3 spherical ionization chambers. The midline dose rate was nominally 3.8 Gy/min based on a midline tissue-to-air ratio of 0.90 applicable for a nominal diameter of 12.6 cm (6). Dose delivery was verified by TLDs irradiated on the entrance and exit surfaces of each animal. Results shown in Table I indicate a remarkably constant

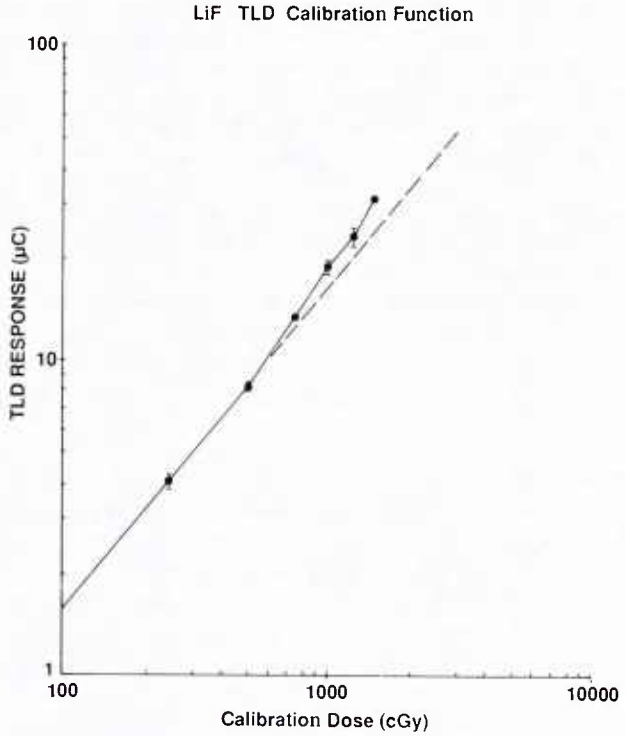

FIG. 2. Calibration curve for TLDs. Each point represents the average of four TLDs. The doses measured in this study of GI damage fall in the range where significant LiF supralinearity occurs. Separate calibration curves were run for each new set of experiments. Error bars represent 1 SD.

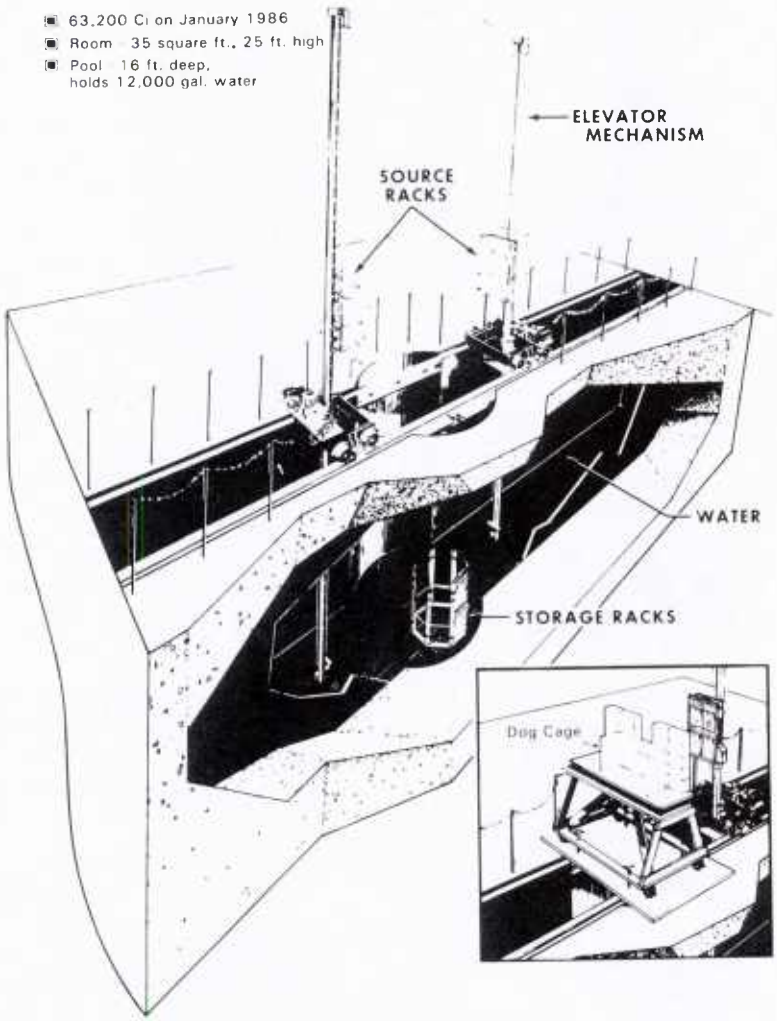

FIG. 3. ^{60}Co Whole Body Irradiation Facility. The main figure shows the facility configuration for routine bilateral exposure (*5*). The inset shows the unilateral irradiation arrangement used in the experiments reported here. The 5-cm-thick Pb bricks shielded the pelvis, spine, and other bones to minimize hematopoietic radiation damage.

ratio (average = 2.12:1) between entrance and exit doses in the first series of animals irradiated in these experiments.

Partial body shielding was provided for each canine by using 5-cm-thick Pb bricks to restrict the radiation field to the area of the intestinal tract (inset, Fig. 3). The resulting ^{60}Co beam exposing the canine gut was approximately 24 cm (width) × 40 cm. The 5-cm bricks attenuated the ^{60}Co intensity by a factor of over 90%. Because of scatter and penumbra effects at the edges of the shields, the dose to some regions of the spine and pelvis was 7 to 10% of the dose at the midline of the open field; other regions of bone marrow received doses less than 7% of nominal midline dose. This shielding was sufficient to allow evaluation of direct GI radiation damage without the influence of concurrent lethal damage to the blood-forming organs.

RESULTS

This *in vivo* TLD dosimetry system allowed measurement of the ^{60}Co dose deposited in the canine small intestine at known distances from the ileostomy. Figure 5 shows dorsal–ventral radiographs of dosimetry tubes in canines just prior to irradiation. Figure 6 shows lateral radiographs of the same animals. The path of the dosimetry tubes is enhanced in each image to show its course through the intestine. It is clear that the position of any specific site along the small intestine is unique for each animal. These radiographs indicate that the radiation dose delivered to specific sites along the intestine cannot be predicted on the basis of external dosimetry measurements or calculations. Only by *in vivo* measurements was it possible to specify the dose for anatomical correlation with endoscopy or other measures of biological damage.

Figure 7 shows the measured ^{60}Co dose as a function of distance from the stoma in the same animals seen in Figs. 5 and 6. The dose was determined from the median TLD reading in each group, with error bars indicating the range. The measured dose profiles varied by a factor of almost two; these variations were in general agreement with the lateral depth of penetration as judged from the dorsal–ventral ra-

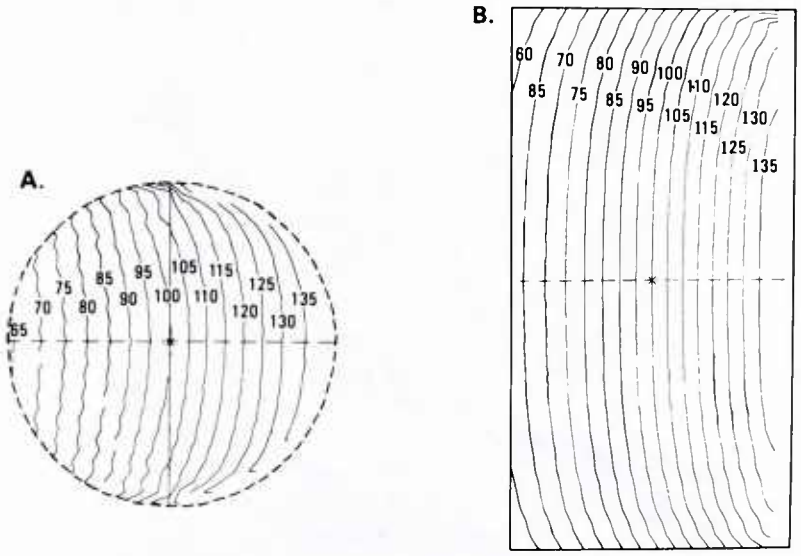

FIG. 4. Calculated ^{60}Co isodose distributions in a cylindrical water phantom. Numerical values give the radiation dose as a percentage of the midline dose. Calculations were for a 15-cm-diameter phantom 32 cm in length.

diographs. However, an exact correlation of dose with depth was not expected, on the basis of the variable heights of the TLD locations as judged from the lateral radiographs. More precise correlations would require a three-dimensional localization of the dosimeters and a three-dimensional outline of each animal. Fortunately the ^{60}Co radiation doses measured by the *in vivo* thermoluminescent dosimetry tube can provide all the information required for radiobiological studies along the length of the intestine.

TABLE I
Entrance–Exit Dosimetry for Canines Unilaterally Irradiated with ^{60}Co

Animal no.	Nominal dose (Gy)	Entrance dose (Gy)	Exit dose (Gy)	Entrance to exit ratio	Weight (kg)
1	10.00	12.38	5.61	2.21	13.3
2	10.00	12.05	5.32	2.27	14.4
3	10.00	12.05	6.45	1.87	12.7
4	10.00	12.65	6.37	1.99	11.6
5	10.00	12.63	6.04	2.09	14.6
6	10.00	12.30	6.14	2.00	14.2
7	10.00	12.34	5.89	2.10	14.2
8	10.00	12.77	6.22	2.05	12.7
9	10.00	13.34	5.96	2.24	11.3
10	10.00	12.42	5.56	2.23	14.6
11	10.00	12.89	6.20	2.08	13.8
12	10.00	12.75	6.37	2.00	9.7
13	10.00	12.53	5.94	2.11	11.3
14	10.00	12.16	6.02	2.02	12.7
15	10.00	12.64	5.78	2.19	12.4
16	10.00	11.53	5.71	2.02	15.1
17	10.00	11.02	4.16	2.65	14.2
18	10.00	12.35	5.71	2.16	12.7
19	15.00	17.10	8.25	2.07	15.2
20	15.00	17.88	8.79	2.03	15.7

Note. Average ratio, 2.12; standard deviation ±7%.

Figure 8 shows the relationship between the average of the radiation doses measured by the TLDs within the intestine of each animal and the nominal or midline doses delivered to that animal. Each point in Fig. 8 represents results for a single animal. The data show that the measured dosimetry results are dispersed within a band ±20% above and below the nominal doses. These results imply that the nominal or midline dose does not characterize the average absorbed dose within the intestine precisely.

In several animals for which both pre- and postirradiation radiographs were made, changes in the position of the small intestine were observed (see Fig. 9). These changes were attributed either to the handling of the canine's restraint box during transport to and from the irradiation facility or to the natural movement of the unanesthetized animal within the restraint box. However, the TLDs were in place *in vivo* during the time of irradiation, so the measured doses accurately reflect the absorbed dose to the intestinal wall at the known distances from the stoma. Movement of the intestines before or after irradiation does not affect the accuracy of the dosimetry results or of the dose-location correlations.

It was also observed that if a dosimetry tube was removed and then reinserted, the final path followed by the small intestine differed appreciably from the original path. This finding emphasized the transient path and location of specific sites along the small intestine.

To correlate dosimetric and endoscopic results reliably, it was necessary to assume that the small intestine did not stretch unreasonably during sequential insertions of the endoscope or the dosimetry tube. The validity of this assump-

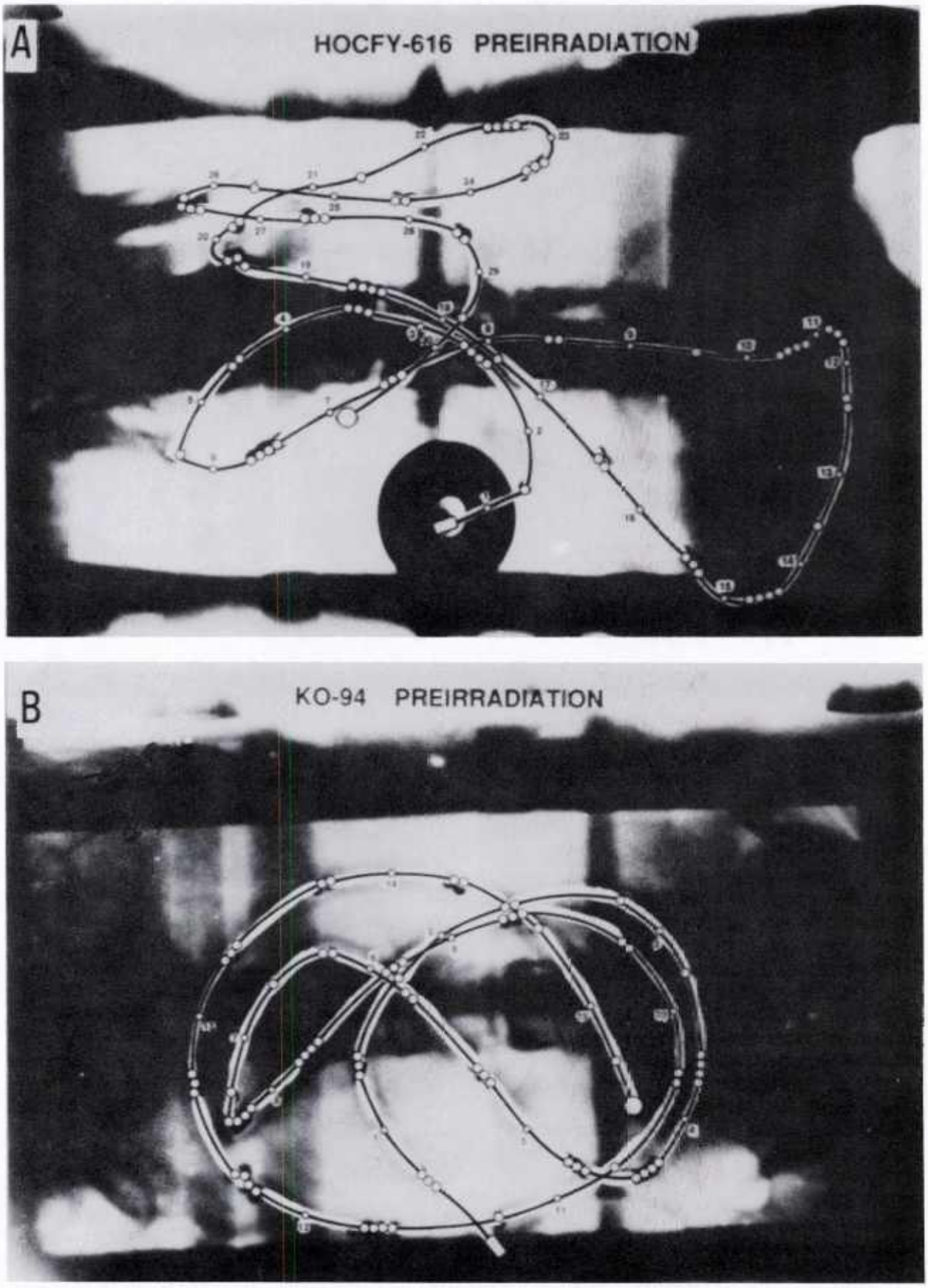

FIG. 5. Dorsal–ventral radiographs of the *in vivo* dosimetry tube in two different animals. The dosimetry tube has been highlighted to accentuate its path within the intestine. Numbers along the paths of the tubes refer to TLD locations; see Fig. 8 for corresponding radiation dose values.

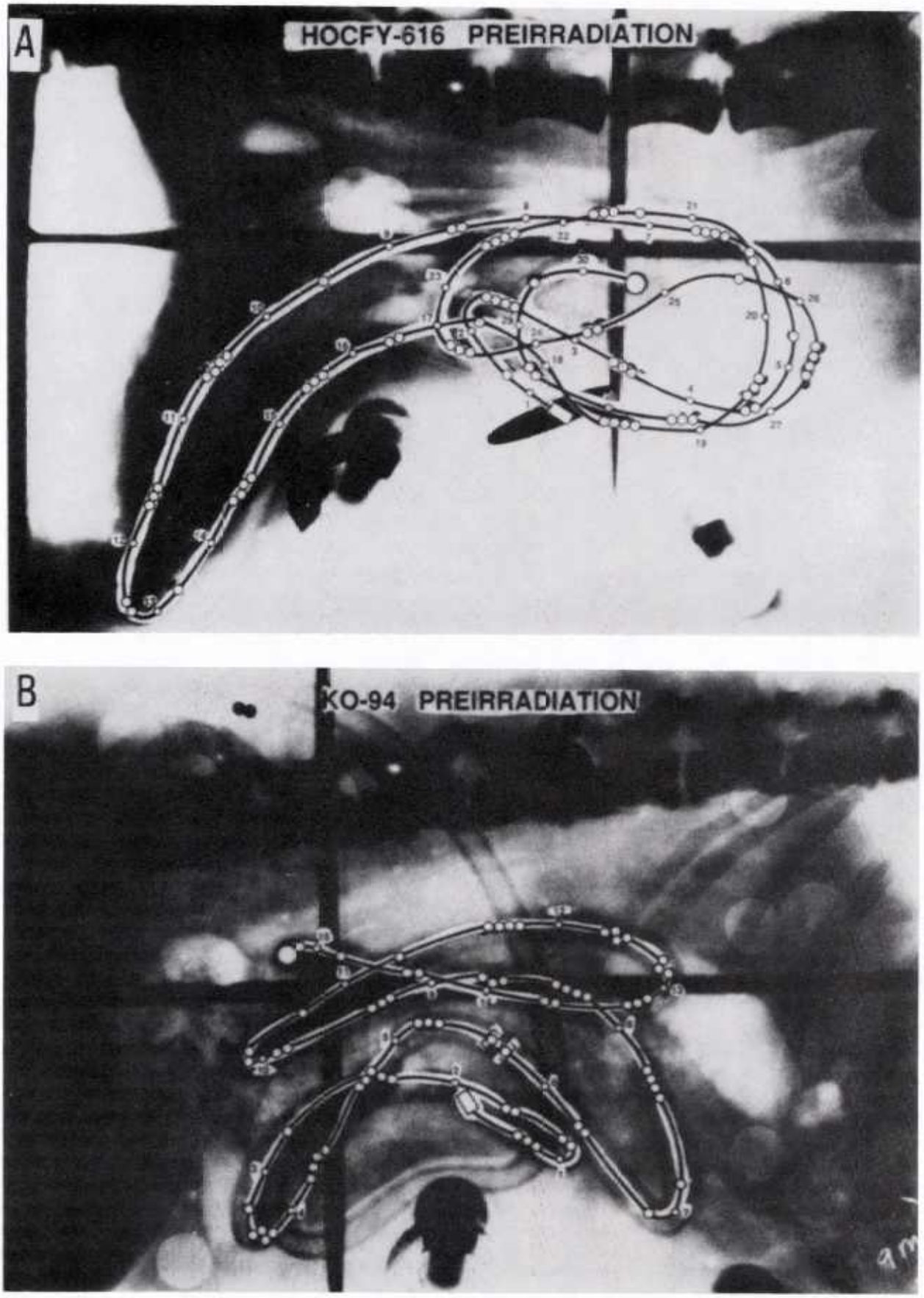

FIG. 6. Lateral radiographs of the *in vivo* dosimetry tube in two different animals. See Fig. 5 for details.

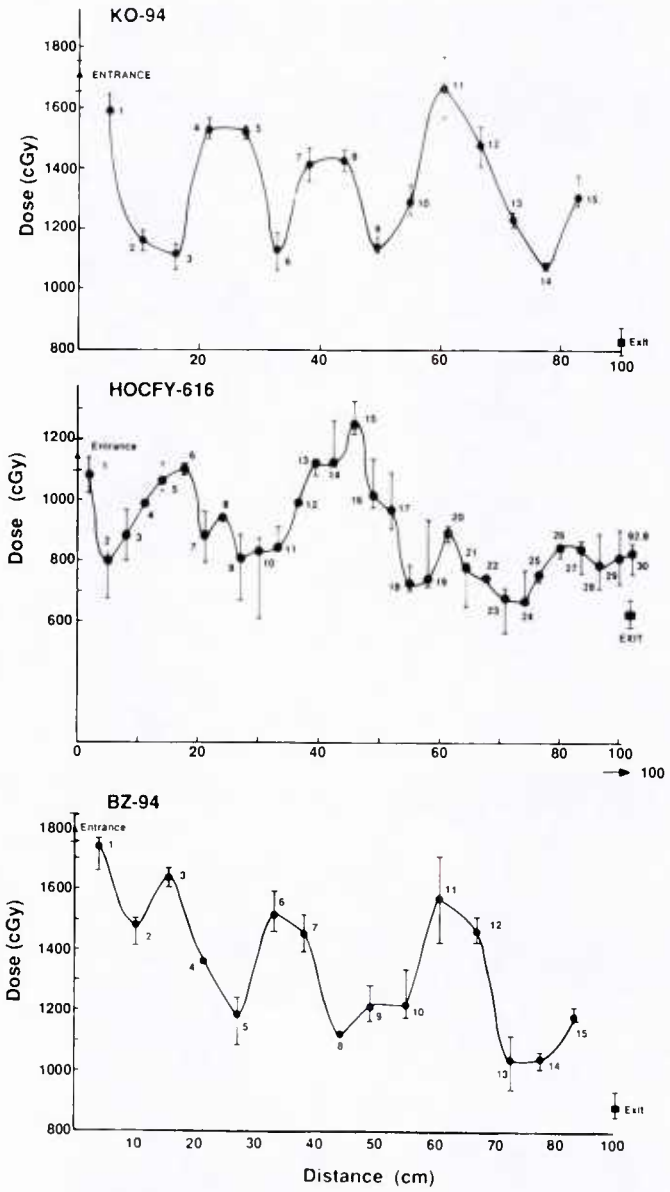

FIG. 7. Measured radiation doses along the length of the dosimetry tube for three different animals. The distance scale refers to distance along the path of each dosimetry tube. The entrance and exit doses plotted on each graph refer to measurements made with separate TLDs positioned on the external surfaces of each animal. Error bars represent range of data.

tion was tested in a control animal by means of fluoroscopy. The endoscopy tube was inserted (nominally 30 cm) until it reached the only reproducible landmark available, namely the surgical anastomosis, and the exact distance was noted. After the endoscopy tube was removed, the dosimetry tube was inserted an equal distance into the intestine. A thin tube filled with radio-opaque fluid was attached to the dosimetry tube to determine its location. Injection of the fluid was observed under fluoroscopy to result in a split stream, simultaneously entering both branches of the anastomosis. It was concluded from this observation that equal reinsertion of the tubes resulted in equal positioning without significant stretching of the intestine.

Endoscopic examinations were performed by inserting the endoscope to depths where dosimetry measurements had been made. The examinations consisted of visualization of the small intestine as well as tissue biopsies for cultures and further analyses as reported in the companion paper (*4*).

DISCUSSION

The experimental model described in this paper facilitates quantitative studies of radiobiological damage to the small intestine following partial-body nonuniform irradiation. The model may be used to obtain intraintestinal dosimetry results from a living animal, and biological observations and samples from specific intestinal sites may be taken at any time before and after irradiation. Thus each animal serves as its own control and provides a complete time course of radiobiological damage and repair. *In vivo* dose measurements make it possible to specify the absorbed dose precisely at locations along the nonuniformly irradiated small intestine. The nonuniform irradiation assures that the absorbed radiation dose varies by a factor of roughly two through regions of the small intestine in each animal. Biological samples from specific locations within the intestine may be directly correlated with the associated radiation dose.

The dosimetry studies reported here emphasize that the movement of the small intestine varies greatly from animal to animal; within an animal, the intestine was also found to change location. A reasonable correlation was generally

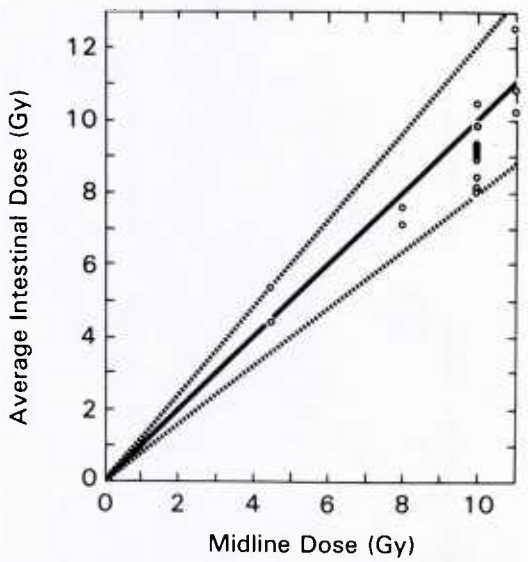

FIG. 8. Correlation of average canine intestinal dose with midline dose. Each point represents the average of all TLD readings from an individual animal. The dashed lines show a ±20% response range above and below the midline dose.

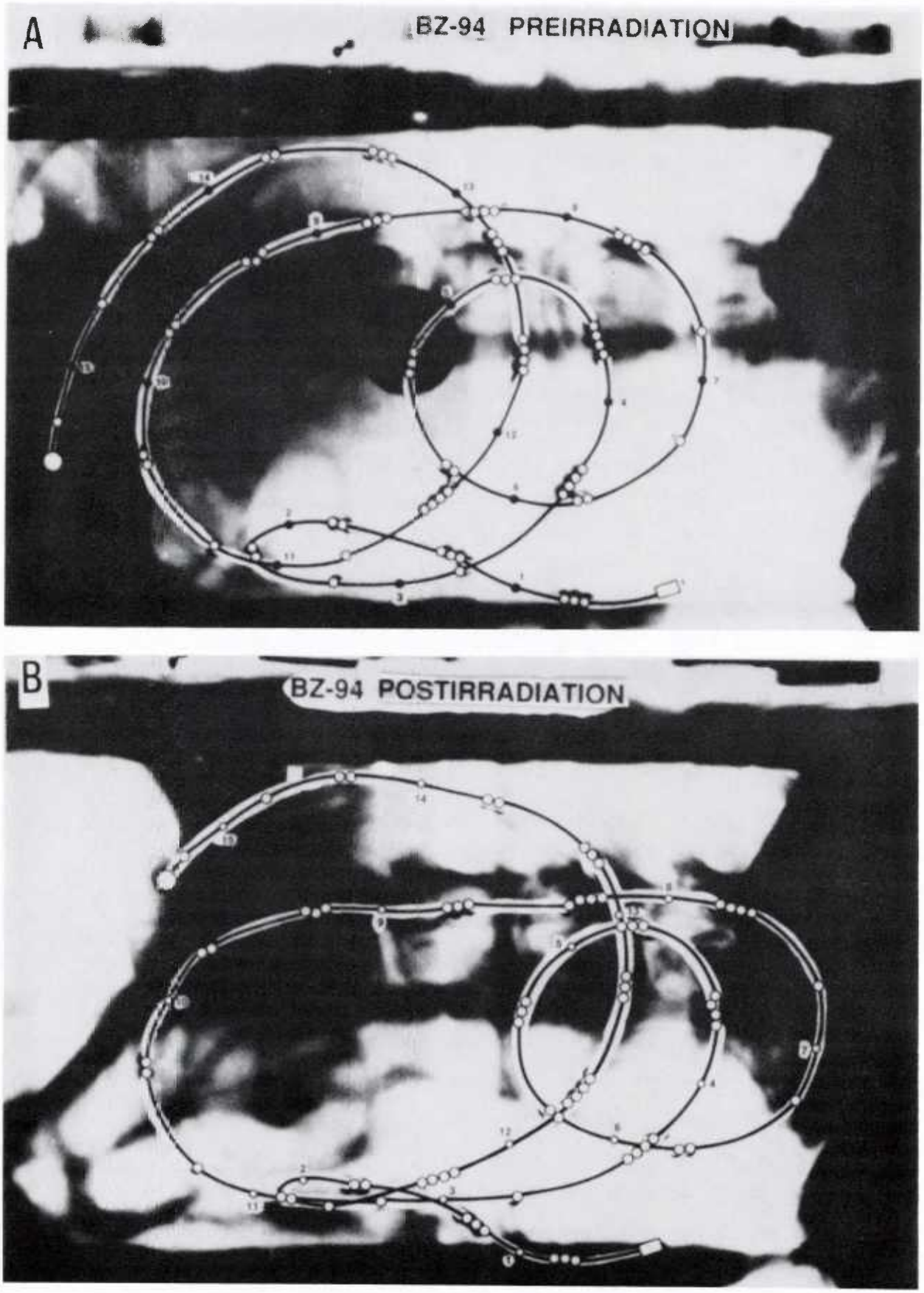

FIG. 9. Pre- and postirradiation dorsal–ventral radiographs of the same animal showing the changed configuration of the dosimetry tube (e.g., note the different locations of the round marker on the distal end of the tube).

observed between measured dose distributions and antieipated doses based on radiographie positions of the dosimeters. However, these comparisons were complicated by the possible movement of the intestine (and the dosimeters) between the time of irradiation and recording of the radiograph and by the aetual three-dimensional loeation of the dosimeters relative to the animal's surfaee eontour. The above observations are consistent with the broad variability (±20%) observed between eaeh animal's average TLD dose and the value of the nominal midline radiation dose. This variability implies that radiosensitive regions of the intestine may be more or less heavily irradiated in individual animals depending on the preeise loeation of the intestine within eaeh animal at the time of irradiation. These findings made it elear that external dosimetry measurements or ealeulations eannot reliably prediet the radiation dose at speeifie sites along the small intestine.

It was demonstrated that the elastie properties of the small intestine were sueh that sequential penetrations of the ileostomy at equal distanees eaused the dosimetry tube or endoseope to reach the same loeation within the intestine. This reproduеibility was essential to efforts to eorrelate measured radiation doses with subsequent endoseopie findings and to assure that sequential samples are taken from the same site at the different times after irradiation.

Extension of the dosimetry techniques deseribed in this paper eould be applied to other large animals or to other radiation sourees. This ability to deseribe quantitatively the radiation dose deposition and radiobiologieal damage along the length of the intestine is being used in the evaluation of new therapeutie proeedures to improve survival following nonuniform irradiation.

ACKNOWLEDGMENTS

This research was supported by the Armed Forces Radiobiology Research Institute, Defense Nuclear Agency, under Work Units 107, B3131, and B5137. The opinions and assertions contained herein are those of the authors; no endorsement by the Defense Nuclear Agency has been given or should be inferred. The experiments reported herein were conducted according to the principles set forth in the "Guide of the Care and Use of Laboratory Animals," Institute of Animal Resources, National Research Council, DHEW Publication No. (NIH) 78-2.

RECEIVED: March 27, 1989; ACCEPTED: August 8, 1989

REFERENCES

1. K. F. BAVERSTOCK and P. J. N. D. ASH, A review of radiation accidents involving whole body exposure and the relevance to the $LD_{50/60}$ for man. *Br. J. Radiol.* **56,** 837–849 (1983).
2. ICRU, *Quantitative Concepts and Dosimetry in Radiobiology,* Report 30. International Commission on Radiation Units and Measurements, Washington, DC, 1979.
3. J. ZOETELIEF, L. A. HENNEN, and J. J. BROERSE, Some practical aspects and dose specification for the whole body irradiation. In *Response of Different Species to Total Body Irradiation* (J. J. Broerse and T. J. MacVittie, Eds.). Nijhoff, Dordrecht, The Netherlands, 1984.
4. R. M. VIGNEULLE, J. HERRERA, T. GAGE, T. J. MACVITTIE, P. L. TAYLOR, G. H. ZEMAN, J. B. NOLD, and A. DUBOIS, Nonuniform irradiation of the canine intestine. I. Effects. *Radiat. Res.* **121,** 46–53 (1990).
5. R. E. CARTER and D. M. VERRELLI, *AFRRI Cobalt Whole-body Irradiator,* Technical Report TR 73-3. Armed Forces Radiobiology Research Institute, Bethesda, MD, 1973.
6. G. H. ZEMAN, M. DOOLEY, and K. WORKING, *Use of a Radiotherapy Treatment Planning Computer for Dosimetry of the AFRRI Cobalt-60 Facility,* Technical Report TR 84-5. Armed Forces Radiobiology Research Institute, Bethesda, MD, 1984.